Key role of retardation and non-locality in sound propagation in amorphous solids as evidenced by a projection formalism

Christiane Caroli, Anaël Lemaître

The Journal of Chemical Physics ARTICLE scitation.org/journal/jcp

Key role of retardation and non-locality in sound propagation in amorphous solids as evidenced by a projection formalism

Cite as: J. Chem. Phys. 153, 144502 (2020); doi: 10.1063/5.0019964
Submitted: 26 June 2020 • Accepted: 16 September 2020 •
Published Online: 13 October 2020

Christiane Caroli[1] and Anaël Lemaître[2,a)]

AFFILIATIONS

[1]Sorbonne Universités, UPMC Université Paris 06, CNRS-UMR 7588, Institut des NanoSciences de Paris, 4 Place Jussieu, 75005 Paris, France

[2]NAVIER, UMR 8205, École des Ponts ParisTech, IFSTTAR, CNRS, UPE, Champs-sur-Marne, France

[a)]**Author to whom correspondence should be addressed:** anael.lemaitre@enpc.fr

ABSTRACT

We investigate acoustic propagation in amorphous solids by constructing a projection formalism based on separating atomic vibrations into two, "phonon" (P) and "non-phonon" (NP), subspaces corresponding to large and small wavelengths. For a pairwise interaction model, we show the existence of a "natural" separation lengthscale, determined by structural disorder, for which the isolated P subspace presents the acoustic properties of a nearly homogenous (Debye-like) elastic continuum, while the NP one encapsulates all small scale non-affinity effects. The NP eigenstates then play the role of dynamical scatterers for the phonons. However, at variance with a conjecture of defect theories, their spectra present a finite low frequency gap, which turns out to lie around the Boson peak frequency, and only a small fraction of them are highly localized. We then show that small scale disorder effects can be rigorously reduced to the existence, in the Navier-like wave equation of the continuum, of a generalized elasticity tensor, which is not only retarded, since scatterers are dynamical, but also non-local. The full neglect of both retardation and non-locality suffices to account for most of the corrections to Born macroscopic moduli. However, these two features are responsible for sound speed dispersion and have quite a significant effect on the magnitude of sound attenuation. Although it remains open how they impact the asymptotic, large wavelength scaling of sound damping, our findings rule out the possibility of representing an amorphous solid by an inhomogeneous elastic continuum with the standard (i.e., local and static) elastic moduli.

I. INTRODUCTION

Glasses and amorphous solids present generic low-temperature thermal and acoustic properties, which are recognized to be signatures of their defining feature: topological structural disorder. However, up to now, no systematic theoretical framework is available to understand how the disordered structure, the details of which depend, e.g., on the degree of relaxation of the glass, determines physical properties such as sound propagation. In the case of systems with weak structural disorder, such as due to dilute point defects in periodic lattices, one can straightforwardly identify a zeroth-order homogeneous state, and hence represent disorder by some scattering potential. In glasses, no systematic method is available to perform such a separation.

Two main types of approaches—defect models[1] and fluctuating elasticity[2]—have been developed[3] to describe the linear vibrational response that controls heat and sound propagation in these systems (except at very low temperatures where quantum effects become relevant[4–6]).

Defect models[1] view a glass as a homogeneous elastic continuum embedding low frequency local oscillators that couple to the continuum via its local strain. This picture is undoubtedly insightful, since glasses are documented to exhibit small soft regions, but remains heuristic in the absence of any clear connection with the

microscopic problem, which raises various questions. For instance, the elastic coupling between oscillators with distributed bare frequencies produces unstable modes, a problem cured by assigning a central role to anharmonicity. It also remains unspecified how these coupled oscillators interact with the embedding continuum to produce, in fine, the modes of the full system and, in particular, the acoustic ones.

Fluctuating elasticity (FE)[2] assumes that the effect of structural disorder on the vibrational properties can be captured by modeling glasses as elastic continua with space-dependent local elastic moduli. Its formulation by Schirmacher *et al.*, hampered by the absence of connection between these moduli and the microscopic problem, considers that the elasticity tensor reduces to fluctuating Lamé constants, the correlations of which are assumed to decay exponentially in space. It predicts the damping coefficients $\Gamma_{L,T}$ to obey the Rayleigh scaling $\sim k^{d+1}$ (with d being the space dimension and k being the wavevector), while numerical[7–10] and experimental[11–17] data support the existence of a regime where attenuation scales as $-k^{d+1}\ln k$,[10] possibly limited toward low frequencies[18,19] by a crossover to a final Rayleigh regime. Recently, we have been able to derive FE from a small wavevector approximation of the microscopic problem, which yields a complete specification of all the fluctuating elasticity coefficients and captures their long-range correlated nature. Contrary to our hope that it would permit us to capture the anomalous scaling of damping, we found that this fully tensorial FE theory predicts, again, the Rayleigh law over the whole wavevector domain where the non-Rayleigh behavior is observed and that it grossly underestimates attenuation. Meanwhile, it yields sound speeds that are only marginally smaller than their (over-)estimates from the Born approximation, which completely neglects non-affine effects. Since FE correctly describes the long wavelength part of the scattering matrix only, these failures demonstrate the crucial role of small scale non-affinity.

This points out to the need for an approach that, instead of tackling separately the local and long-range aspects of disorder, as done by defect theories and FE, respectively, would permit us to combine their effects. Such an attempt was proposed by Schirmacher and Maurer[3] who built a model in which the FE elastic continuum is coupled with the local oscillators. They adopt the assumptions of phenomenological defect theories both concerning the properties of local oscillators and their coupling, via local strain, with the continuum. This extended theory, again, predicts the standard, rather than the observed, anomalous, Rayleigh scaling for attenuation.

Clearly, to model acoustic propagation, it is necessary to construct a representation of a glass as an elastic continuum coupled with small scale scatterers. The failure of phenomenological approaches to predict the observed acoustic properties shows that we do not yet know how to do so while specifying consistently both the nature of scatterers and the form of their coupling with the continuum. To overcome this issue, one needs to assess how such a representation can be derived from the microscopic wave equations.

Here, we endeavor to do so by constructing a projection formalism that separates vibrational atomic displacements into large and small scale contributions. For this purpose, we define the "phonon" (P) sub-space as the space generated by all discrete plane waves with wavevectors up to an upper cutoff k_c. Its orthogonal complement is called the "non-phonon" (NP) sub-space. Decomposing the Hessian of the microscopic problem on these two sub-spaces enables us to identify the zeroth order of the scattering problem as its restriction to its block-diagonal part, which defines two uncoupled P and NP problems.

Implementing this formalism numerically for a 2D soft sphere model, we show that the whole spectrum of the phonon subspace is quasi-Debye, with sound speeds achieving their Born values, as long as k_c remains smaller than a rather large, finite value $k_c^{\max}$ corresponding to a few interatomic distances. This brings evidence that there exists a natural scale below which the non-affine effects are concentrated. When choosing k_c close to this upper limit, we effectively restrict the NP part to small scales, thus fulfilling our objective to represent the amorphous solid as an elastic continuum (the P subspace) perturbed by the non-affine effects at small scales (captured by the NP part). It is the existence of such a separation scale that justifies the relevance of the projection formalism. Moreover, it is worth mentioning that this separation scale turns out to lie close to the Boson peak length[20–22] that was proposed to be a measure of the size of elastic heterogeneities.

In this description, the eigenmodes of the NP problem act as scatterers for the bare P states, which couple via the off-diagonal part of the Hessian. In qualitative agreement with the defect picture, the low lying NP states present a high degree of localization; however, at odds with the assumptions of these models, we find that the NP spectrum does not extend down to zero frequency but, as required by the well-posedness of the full (recoupled) problem, presents a *finite low energy gap*, which turns out to be of the order of the Boson peak frequency. This gap value guarantees a large overlap between the P and NP spectra, hence suggesting an efficient P–NP coupling. Thus, our approach directly demonstrates that attenuation results from the coupling of phonons with small-scale scatterers, with energies that are broadly distributed, yet with a finite lower cutoff.

We then show that the microscopic equations for sound propagation can be rigorously recast into a Navier-like continuum equation, yet with a generalized elasticity tensor that is both non-local and retarded, a feature that reflects that the scattering between two phonon states is mediated by propagation within the NP subspace.

Finally, we analyze in detail the importance of retardation and non-locality. We find that, quite remarkably, their full neglect suffices to explain about 70% of the departure between actual and Born sound speed values in the $k \to 0$ limit. However, we show that it is these two features that are responsible for the downward curvatures of sound speed $c_{L,T}(k)$ curves; we also bring preliminary evidence that their neglect, and especially that of non-locality, leads to a significant underestimate of the magnitude of sound damping and possibly to a scaling different from the observed one. This formalism and the ensuing set of results challenge the idea that the effect of structural disorder on sound propagation can be reduced to the existence of local fluctuating elasticity coefficients; meanwhile, they open the possibility to construct extended elasticity models involving second gradient contributions.

II. PROJECTION FORMALISM

To investigate the acoustic response of a glass, our starting point is the discrete wave equation, linearized about a glassy inherent state,

$$\frac{\partial^2 \mathbf{u}}{\partial t^2} = -\mathcal{H}\mathbf{u}. \tag{1}$$

Here, we consider an inherent state of a glass composed of N atoms of mass $m = 1$, labeled $i = 1, \ldots, N$, occupying a cubic, periodic cell of volume $V = L^d$ in dimension d. We denote $\underline{r}_i = \{r_i^\alpha\}$ as the position of atom i in the inherent state and $\underline{u}_i \equiv \{u_i^\alpha\}$ as its displacement away from $\underline{r}_i$ (greek letters label Cartesian coordinates). The discrete (particle) displacement field, a vector of dimension Nd, is defined as $\mathbf{u} \equiv \{u_i^\alpha\}$. Finally, since the inherent state is by definition stable, the Hessian $\mathcal{H} = \{\mathcal{H}_{ij}^{\alpha\kappa}\}$ is positive definite (except for the translation modes).

We introduce the discrete plane waves $\boldsymbol{\varphi}_{\underline{k},\underline{a}}$ that are the Nd vectors with components,

$$\left(\underline{\varphi}_{\underline{k},\underline{a}}\right)_i = \frac{\underline{a}}{\sqrt{N}} e^{i\underline{k}\cdot\underline{r}_i}, \tag{2}$$

where $\underline{k} = 2\pi\,\underline{n}/L$, with $\underline{n} \equiv \{n^\alpha\}$ being a vector with integer components, and $\underline{a} \equiv \{a^\alpha\}$, a normalized ($|\underline{a}| = 1$) polarization vector. The $\boldsymbol{\varphi}_{\underline{k},\underline{a}}$'s are normalized

$$\left|\boldsymbol{\varphi}_{\underline{k},\underline{a}}\right|^2 \equiv \boldsymbol{\varphi}_{\underline{k},\underline{a}}^\dagger \boldsymbol{\varphi}_{\underline{k},\underline{a}} = 1 \tag{3}$$

for the scalar product of dimension-Nd vectors,

$$\mathbf{u}^\dagger \mathbf{v} = \sum_i \underline{u}_i^* \cdot \underline{v}_i. \tag{4}$$

Note that the dot is used throughout to denote the contraction on the Cartesian indices.

In order to separate large and small scale motions, we choose a cutoff k_c such that the number M of wavevectors of the norm $|\underline{k}| < k_c$ verifies $M \ll N$. We then consider the Md-dimensional space generated by all discrete plane waves with $|\underline{k}| < k_c$, which we call *the phonon subspace* P. We decompose any discrete displacement field $\mathbf{u}$ onto P and its orthogonal complement, which we call *the non-phonon subspace* NP. Specifically, denoting $\mathcal{P}$ as the projection operator onto P, we write

$$\mathbf{u} = \mathbf{u}^{\mathrm{P}} + \mathbf{u}^{\mathrm{NP}}, \tag{5}$$

where $\mathbf{u}^{\mathrm{P}} \equiv \mathcal{P}\mathbf{u}$ and $\mathbf{u}^{\mathrm{NP}} \equiv (\mathbf{1} - \mathcal{P})\mathbf{u}$.

By definition, the phonon part $\mathbf{u}^{\mathrm{P}}$ is a linear superposition of Md plane waves,

$$\mathbf{u}^{\mathrm{P}} = \sum_{\substack{(\underline{k},\underline{a}) \\ k<k_c}} \widehat{u}_{\underline{k},\underline{a}}\, \boldsymbol{\varphi}_{\underline{k},\underline{a}}. \tag{6}$$

To obtain a more compact notation, we combine the Md scalar coordinates $\widehat{u}_{\underline{k},\underline{a}}$ into the (column) vector $\widehat{\mathbf{u}} = \{\widehat{u}_{\underline{k},\underline{a}}\}$ and introduce the $Nd \times Md$ matrix $\boldsymbol{\Phi}$ with the $\boldsymbol{\varphi}_{\underline{k},\underline{a}}$ as columns. It yields

$$\mathbf{u}^{\mathrm{P}} = \boldsymbol{\Phi}\widehat{\mathbf{u}}. \tag{7}$$

Note that, here, $\mathbf{u}^{\mathrm{P}}$ and $\widehat{\mathbf{u}}$ are Nd- and Md-dimensional, respectively.

Let us emphasize that, in general, the discrete plane waves are not mutually orthogonal. Therefore, the component $\widehat{u}_{\underline{k},\underline{a}} \neq \boldsymbol{\varphi}_{\underline{k},\underline{a}}^\dagger \mathbf{u}$.

To obtain an explicit expression for $\mathcal{P}$, we first observe that the Md scalar products $\boldsymbol{\varphi}_{\underline{k},\underline{a}}^\dagger \mathbf{u}$ are the components of $\boldsymbol{\Phi}^\dagger \mathbf{u}$. Accordingly, since the non-phonon part $\mathbf{u}^{\mathrm{NP}}$ lies by definition in the space orthogonal to P, it verifies

$$\boldsymbol{\Phi}^\dagger \mathbf{u}^{\mathrm{NP}} = 0 \tag{8}$$

whence

$$\boldsymbol{\Phi}^\dagger \mathbf{u} = \boldsymbol{\Phi}^\dagger \mathbf{u}^{\mathrm{P}} = \boldsymbol{\Phi}^\dagger \boldsymbol{\Phi}\, \widehat{\mathbf{u}}. \tag{9}$$

Since the set of $\boldsymbol{\varphi}_{\underline{k},\underline{a}}$ forms a basis for P, the matrix $\boldsymbol{\Phi}^\dagger\boldsymbol{\Phi}$ is invertible, and we may write

$$\widehat{\mathbf{u}} = \left(\boldsymbol{\Phi}^\dagger \boldsymbol{\Phi}\right)^{-1} \boldsymbol{\Phi}^\dagger \mathbf{u}. \tag{10}$$

Finally,

$$\mathbf{u}^{\mathrm{P}} = \boldsymbol{\Phi}\left(\boldsymbol{\Phi}^\dagger \boldsymbol{\Phi}\right)^{-1} \boldsymbol{\Phi}^\dagger \mathbf{u}, \tag{11}$$

which yields, for $\mathcal{P}$, the explicit form

$$\mathcal{P} = \boldsymbol{\Phi}\left(\boldsymbol{\Phi}^\dagger \boldsymbol{\Phi}\right)^{-1} \boldsymbol{\Phi}^\dagger. \tag{12}$$

Using this formalism, the wave equation may be decomposed into the phonon and non-phonon subspaces as follows:

$$\begin{aligned} \ddot{\mathbf{u}}^{\mathrm{P}} &= -\mathcal{H}^{\mathrm{P,P}}\mathbf{u}^{\mathrm{P}} - \mathcal{H}^{\mathrm{P,NP}}\mathbf{u}^{\mathrm{NP}}, \\ \ddot{\mathbf{u}}^{\mathrm{NP}} &= -\mathcal{H}^{\mathrm{NP,P}}\mathbf{u}^{\mathrm{P}} - \mathcal{H}^{\mathrm{NP,NP}}\mathbf{u}^{\mathrm{NP}}, \end{aligned} \tag{13}$$

where

$$\begin{aligned} \mathcal{H}^{\mathrm{P,P}} &\equiv \mathcal{P}\mathcal{H}\mathcal{P}, \\ \mathcal{H}^{\mathrm{P,NP}} &\equiv \mathcal{P}\mathcal{H}(\mathbf{1} - \mathcal{P}), \\ \mathcal{H}^{\mathrm{NP,P}} &\equiv (\mathbf{1} - \mathcal{P})\mathcal{H}\mathcal{P}, \\ \mathcal{H}^{\mathrm{NP,NP}} &\equiv (\mathbf{1} - \mathcal{P})\mathcal{H}(\mathbf{1} - \mathcal{P}). \end{aligned} \tag{14}$$

In the rhs of Eq. (13), keeping only the terms associated with the diagonal "blocks," $\mathcal{H}^{\mathrm{P,P}}$ and $\mathcal{H}^{\mathrm{NP,NP}}$, defines a zeroth order problem in which the phonon and non-phonon subspaces are decoupled. Note that both blocks are guaranteed to be positive definite (excluding the two translation modes), since $\mathcal{H}$ is.

This projection scheme is formulated with the objective of separating large and small scale contributions to sound propagation, i.e., of representing an amorphous solid as a (fluctuating) elastic continuum—the phonon subspace—perturbed by small scale non-affine effects—captured by the non-phonon part. To assess whether this program can be realized, we first examine the vibrational properties of the two uncoupled P and NP subspaces, before examining how the recoupling of these two subspaces leads to a Navier-like acoustic wave equation.

We implement this in the case of the two-dimensional binary soft sphere system of Refs. 10 and 23 (particle density $\rho = N/L^2 = 1.6$), using systems comprising $N = 11\,350$, $45\,395$, and $181\,582$ atoms, which correspond to linear sizes $L \simeq 84$, 168, and 337, respectively. Lennard-Jones units are used throughout (see details in Appendix A).

III. THE PHONON SUBSPACE

To characterize the elastic behavior of the isolated phonon subspace and assess the influence of the choice of k_c, we compute sound speeds and attenuation coefficients using the protocol of Refs. 10 and 24. It consists in numerically integrating

$$\ddot{\mathbf{u}}^{\mathrm{P}} = -\boldsymbol{\mathcal{H}}^{\mathrm{P,P}}\,\mathbf{u}^{\mathrm{P}} \tag{15}$$

with the initial condition $\mathbf{u}(t=0)=0$, $\dot{\mathbf{u}}(t=0^+)=\boldsymbol{\varphi}_{\underline{k},a}$ for various $\underline{k}$ vectors of norm $k<k_c$ and for both longitudinal (L) and transverse (T) polarizations. The velocity autocorrelation $\dot{\mathbf{u}}^{\mathrm{P}}(t)\cdot\mathbf{u}^{\mathrm{P}}(0^+)=\dot{\mathbf{u}}^{\mathrm{P}}(t)\cdot\boldsymbol{\varphi}_{\underline{k},a}$ is very well fitted by a damped oscillatory form, which provides frequencies (hence sound speeds) and damping coefficients.

In Fig. 1, we report the resulting sound speeds $c_{\mathrm{L,T}}$ and attenuation coefficients $\Gamma_{\mathrm{L,T}}$, for two system sizes $L=168$ and $L=337$, and three values of $k_c=2\pi\,n_c/L=0.75$, 1.12, and 1.5, which correspond to wavelengths 8.4, 5.6, and 4.2, respectively. For each L, the investigated k values range from k_c down to $k_{\min}=2\pi\,n_{\min}/L$, with $n_{\min}=6$.[25] Like in the full system, the measured values of $c_{\mathrm{L,T}}$ and $\Gamma_{\mathrm{L,T}}$ are size-independent over the considered k range.

Observe that the measured sound speeds remain in all cases close to their values (black lines) in the Born approximation, which fully neglects any non-affinity. Although they are systematically smaller than the Born estimates and increasingly more so as k_c increases (i.e., as the P problem incorporates shorter and shorter wavelengths), this effect is quite weak: when k_c varies by a factor of 2 (from 0.75 to 1.5), the reduction in $c_{\mathrm{L,T}}$ is at most 1% in the $k<0.5$ range (which is much broader than the acoustic domain). This must be put in regard with the 6% and 40% discrepancies between the $k\to 0$ values of c_{L} and c_{T}, respectively, when comparing the Born ($c_{\mathrm{L}}^{\mathrm{Born}}\simeq 8.6$, $c_{\mathrm{T}}^{\mathrm{Born}}\simeq 4.41$) and full problem values ($c_{\mathrm{L}}^{\mathrm{full}}\simeq 8.04$, $c_{\mathrm{T}}^{\mathrm{full}}\simeq 3.17$).

Besides, both attenuation coefficients $\Gamma_{\mathrm{L,T}}$ reach a k_c-independent Rayleigh regime at small k, a scaling behavior that differs from that ($\Gamma_{\mathrm{L,T}}\propto -k^3\ln k$) of the full problem in the same k range. Like in the FE approximation,[23] these values underestimate the full problem attenuation coefficients, as computed in Ref. 10, by at least one order of magnitude.

These observations show that reducing the wave equation to the uncoupled P subspace is grossly insufficient to describe acoustic propagation in amorphous solids as it suffers from the same deficiencies as the FE approximation:[23] sound speed values very close to their Born estimates and much too small attenuation coefficients that, moreover, obey the standard Rayleigh scaling at low k.

The comparison of sound speed and attenuation data in these two approximations in Fig. 2 show that they are, in fact, in very good quantitative agreement. This stems from the fact that, as analyzed in Ref. 23, the FE approximation results from the asymptotic matching of the Hessian $\boldsymbol{\mathcal{H}}$, at long wavelengths, by the functional form of a tensorial continuum elasticity kernel. This procedure relies on linearizing factors of the form $\sin(\underline{k}\cdot\underline{r}_{ij}/2)$, where $\underline{r}_{ij}$ is the vector separating two interacting atoms i, j, which requires $\underline{k}\cdot\underline{r}_{ij}/2\lesssim\pi/6$, i.e., $k\lesssim 1$. This explains why the FE turns out to be a good approximation for the uncoupled P problem, as long as $k_c\lesssim 1$.

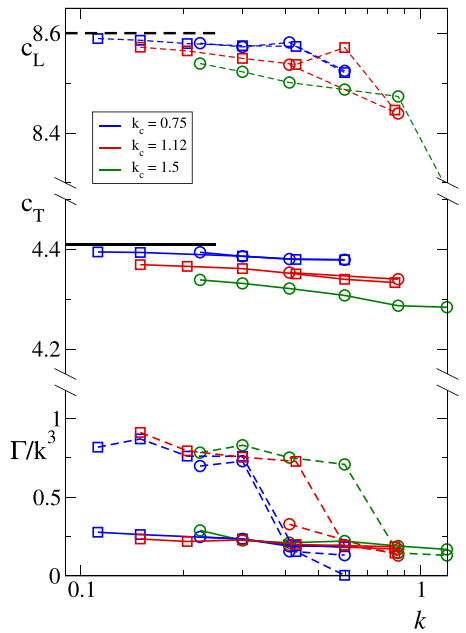

FIG. 1. For the P problem in $L\approx 168$ (circles) and ≈ 337 (squares) systems: longitudinal (dashed) and transverse (solid) sound speeds $c_{\mathrm{L,T}}$ and attenuation coefficients $\Gamma_{\mathrm{L,T}}$ as a function of k. Black horizontal lines correspond to the Born sound speeds.

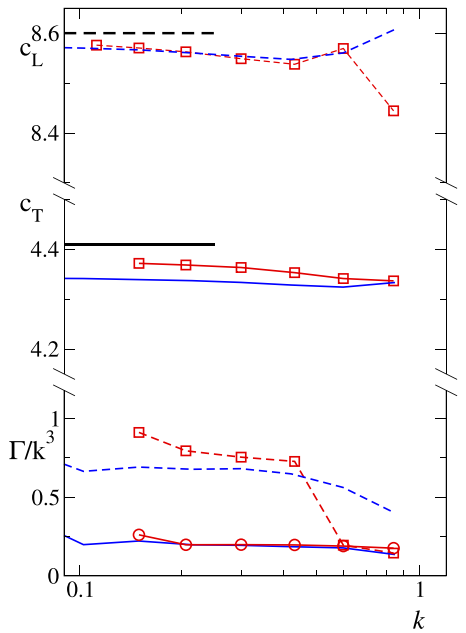

FIG. 2. Longitudinal (dashed) and transverse (solid) sound speeds $c_{\mathrm{L,T}}$ and attenuation coefficients $\Gamma_{\mathrm{L,T}}$ for both the P problem (with $L\simeq 337$, $k_c=1.12$, red squares) and the FE approximation (using $L\simeq 673$, $q_{\max}=1.6$, blue lines). Black horizontal lines: the Born sound speeds.

The weakness of damping in the P problem suggests that its eigenmodes are close to plane waves. To test this idea, we compute its spectrum, which is defined by the eigenvalue equation

$$\mathcal{H}^{\mathrm{P,P}}\,\mathbf{u}^{\mathrm{P}} = \omega^2\,\mathbf{u}^{\mathrm{P}}. \tag{16}$$

To efficiently solve this problem, we rewrite the above equation in terms of the Md-dimensional vector $\widehat{\mathbf{u}} = \{\widehat{u}_{\underline{k},a}\}$ [see Eqs. (6) and (7)]. Using Eqs. (10) and (12), the eigenvalue problem becomes

$$\mathbf{\Phi}^\dagger\mathcal{H}\mathbf{\Phi}\widehat{\mathbf{u}} = \omega^2\,\mathbf{\Phi}^\dagger\mathbf{\Phi}\widehat{\mathbf{u}}, \tag{17}$$

where both matrices $\mathbf{\Phi}^\dagger\mathcal{H}\mathbf{\Phi}$ and $\mathbf{\Phi}^\dagger\mathbf{\Phi}$ are self-adjoint and positive definite. This problem is solved numerically using the generalized eigensolver of the Eigen library.

The density of P states, $\rho^{\mathrm{P}}(\omega)$, is displayed in Fig. 3, as ρ^{P}/k_c vs ω/k_c, for $L = 168$ and 337 and various k_c's. It is compared in this figure with the density of the Debye spectrum of an infinite continuum, restricted to $k < k_c$ plane waves

$$\rho^{\mathrm{D}}(\omega) = \begin{cases} \frac{1}{2\pi}\left(\frac{1}{c_{\mathrm{T}}^2} + \frac{1}{c_{\mathrm{L}}^2}\right)\omega & \text{for } \omega < c_{\mathrm{T}}\,k_c \\ \frac{1}{2\pi\,c_{\mathrm{L}}^2}\,\omega & \text{for } \omega \in [c_{\mathrm{T}}\,k_c, c_{\mathrm{L}}\,k_c] \end{cases} \tag{18}$$

using for $c_{\mathrm{L,T}} = c_{\mathrm{L,T}}^{\mathrm{Born}}$ the Born sound speeds.

The ρ^{P} data are, as anticipated, very close to the Debye density of states (DOS), which confirms that the P subsystem can be viewed as a nearly homogeneous elastic continuum in which sound speeds have their Born values.

Note incidentally that, in Fig. 1, the k_c-dependent drop in Γ_{L} occurs at a wavenumber $\simeq k_c\,c_{\mathrm{T}}^{\mathrm{Born}}/c_{\mathrm{L}}^{\mathrm{Born}}$, which corresponds to the frequency $\simeq k_c c_{\mathrm{T}}^{\mathrm{Born}}$ where the Debye DOS presents its first discontinuity, associated with the disappearance of transverse phonons. In the P problem, the height of the Γ_{L}/k^3 plateau at very long wavelengths $k < k_c\,c_{\mathrm{T}}^{\mathrm{Born}}/c_{\mathrm{L}}^{\mathrm{Born}}$ thus points out to the existence of couplings between longitudinal and transverse waves.

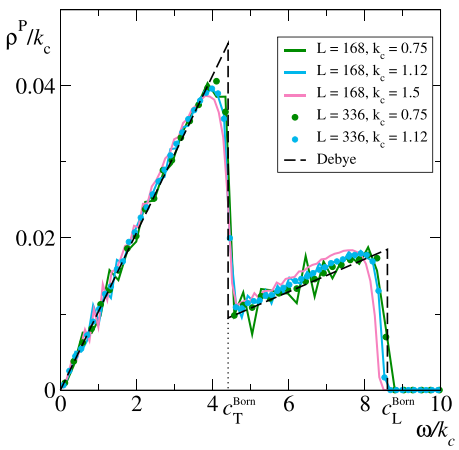

FIG. 3. Density of P states (colors) for system size $L = 168$ (solid lines), for different k_c values, and $L = 337$ (circles) for $k_c = 0.75$. Black dashed line: the Debye density of state using the Born approximation for elasticity.

We analyzed $L \simeq 84$ (not shown), 168, and 337 data and found no size effect except for the fact that smaller L and/or k_c data present larger fluctuations that are not eliminated with an improved statistical sampling. This can be seen in Fig. 3, where the $k_c = 0.75$ data for the two considered system sizes track each other, but the $L \simeq 168$ one, even though it averages many more configurations, presents a higher degree of fluctuations. This size effect is an additional signature of the weakness of the scattering induced by long wavelength disorder only. Indeed, single configurations present spectra that closely follow the level structure expected for a homogeneous continuum. The disorder-induced broadening is too small to smooth out the peaks of the Debye density of state at the lowest k's in these finite-sized systems.

Consistent with the trend shown by the sound propagation data, ρ^{P} progressively departs from the Debye density with increasing k_c. This shows up via

(a) a weak and gradual increase in the slopes, which corresponds to the slight decrease in sound velocities; and
(b) a progressive rounding off close to the two discontinuities of the Debye DOS where the modes primarily combine phonons with k lying near the upper edge of the P sub-space.

Note that above $c_{\mathrm{T}}^{\mathrm{Born}}$, the departure between the $k_c = 0.75$ and 1.12 curves is quite small and of the order of our fluctuations. In contrast, the $k_c = 1.5$ data are almost twice as far from the Debye prediction than the $k_c = 1.12$ one. Hence, the P spectrum starts to very sensitively depart from the Debye one for k_c values beyond about 1 or 1.12, which is therefore rather sharply defined.

The above analysis clearly documents the following:

(i) The P spectrum is essentially independent of k_c so long as $k_c \lesssim 1$—which is the condition needed for the linearization of the $\sin(\underline{k}\cdot\underline{r}_{ij}/2)$ factor in the small-k expansion of the Hessian.
(ii) Under this condition, unlike the full system, the P sub-problem can be viewed as equivalent to a very weakly inhomogeneous elastic continuum restricted to long wavelengths.
(iii) The long wavelength part of disorder is grossly insufficient to account for acoustic attenuation, which confirms that the coupling between the P and NP subspaces cannot be ignored.

Moreover, points (i) and (ii) lead to an important conclusion. Since, in order to optimally separate the P and NP parts, one should choose k_c as large as possible within the allowed range, they entail that the value of k_c is not an arbitrary parameter but is imposed by the nature of atomic interactions. It thus emerges that, for a given disordered system, *there exists a "natural" scale of separation between short and long wavelengths*.

IV. THE NON-PHONON SUBSPACE

Solving directly the NP eigenvalue problem

$$\mathcal{H}^{\mathrm{np,np}}\,\mathbf{u}^{\mathrm{np}} = \lambda\,\mathbf{u}^{\mathrm{np}} \tag{19}$$

requires constraining $\mathbf{u}^{\mathrm{np}}$ to the NP space, which is computationally inefficient since we cannot identify a basis for the NP space, hence

cannot explicitly reduce the problem to a $(N - M)d$-dimensional NP space. Instead, we solve the same problem as above, but in the full Nd-dimensional space of discrete displacements,

$$\mathcal{H}^{\mathrm{np,np}}\,\mathbf{u} = \lambda\,\mathbf{u}, \tag{20}$$

and then sort out the eigenmodes we look for. For this purpose, we note the following:

(a) Any element of P is a $\lambda = 0$ eigenvector of $\mathcal{H}^{\mathrm{np,np}}$.
(b) $\mathcal{H}^{\mathrm{np,np}}$, when restricted to the NP subspace [problem (19)], is positive definite because it is a diagonal subblock of $\mathcal{H}$, which is itself positive definite; its $(N - M)d$ eigenvalues are hence all strictly positive.
(c) Any of the $(N - M)d$ eigenvector–eigenvalue pairs for problem (19) also verifies problem (20).

It follows that the $\lambda = 0$ eigenspace of problem (20) is the phonon subspace, while all its non-zero eigenmodes, since they are orthogonal to P, generate the NP space.

We solve (20) using the standard LAPACK algorithm for real, symmetric matrices. It requires storing the upper triangular part of $\mathcal{H}^{\mathrm{np,np}}$, as expressed in the full Nd-dimensional space of all atomic displacements, which limits the calculation to system sizes up to $L \simeq 168$.

The ensemble-averaged NP DOS is shown in Fig. 4 for two system sizes ($L \simeq 84$ and 168) and three values of k_c. For a given k_c, as can be expected when $L \gg 2\pi/k_c$, the NP DOS's are size-independent. Their most conspicuous feature is the presence of a finite low frequency gap ω_g, which increases with k_c. The inset of Fig. 4 additionally shows that $\omega_g \propto k_c$ in the $k_c \in [0.75, 1.5]$ range of interest, a point we will later come back to.

By construction, the NP subspace contains all small-scale non-affine contributions to atomic displacements. Its modes act as a set of oscillators that, in the full problem, couple with phonon modes, thus giving rise to sound scattering.

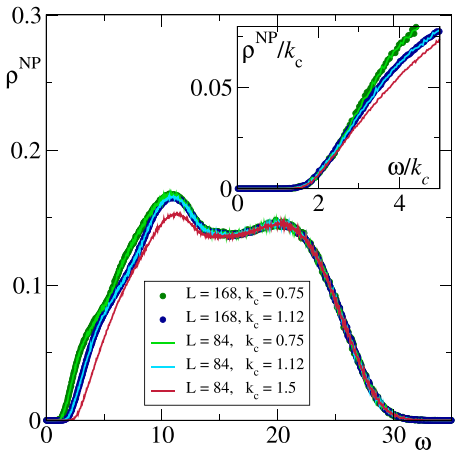

FIG. 4. Density of NP states (colors) for system size $L \simeq 84$ (solid lines) and 168 (circles) for different k_c values. (Inset) A zoomed-in view of the low frequency gap.

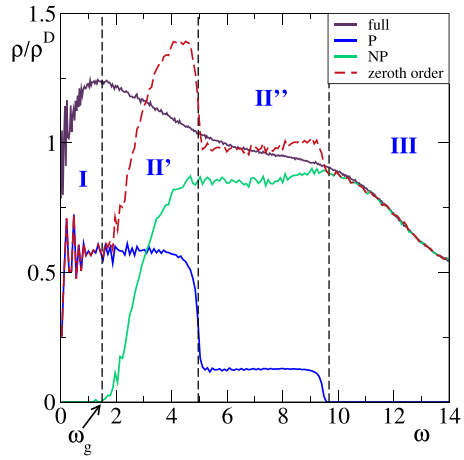

FIG. 5. For $k_c = 1.12$, the ratios $\rho^{\mathrm{P}}/\rho^{\mathrm{D}}$ (blue, $L = 337$), $\rho^{\mathrm{NP}}/\rho^{\mathrm{D}}$ (green, $L = 168$), and their sum $\rho^{(0)}/\rho^{\mathrm{D}}$ (red, dashed), compared with $\rho^{\mathrm{full}}/\rho^{\mathrm{D}}$ (brown, $L = 673$).

At zeroth order in the P–NP coupling, the full problem is the superposition of the uncoupled P and NP subproblems, and its density of states is $\rho^{(0)} = \rho^{\mathrm{P}} + \rho^{\mathrm{NP}}$. To gain insight into the nature and importance of P–NP coupling effects in different frequency domains, we compare in Fig. 5, for a given k_c, ρ^{P}, ρ^{NP}, and $\rho^{(0)}$, with the full problem DOS ρ^{full}. We use here the value of $k_c \simeq 1.12$, which, in Sec. III, appeared to be in the optimal range of P–NP separation. In this plot, all distributions are normalized by the Debye density of states $\rho^{\mathrm{D}}(\omega)$ computed with the full problem sound speeds. As expected, $\rho^{\mathrm{full}}/\rho^{\mathrm{D}}$ exhibits a Boson peak, which lies about $\omega_{\mathrm{BP}} \simeq 1.3$.

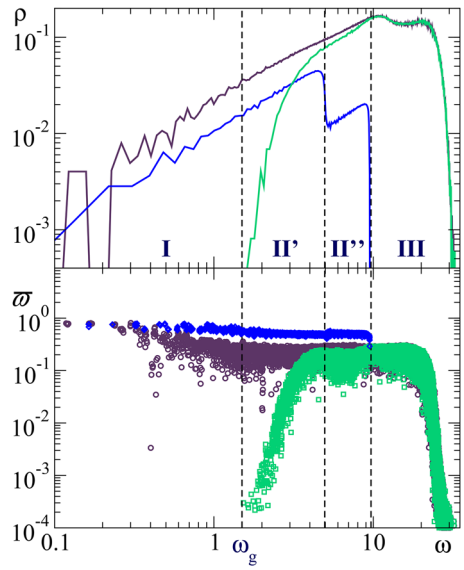

FIG. 6. P, NP, and full problem spectra for $k_c = 1.12$. (Top) DOS for the P (blue, $L = 337$), NP (green, $L = 168$), and full problems (brown, $L = 673$). (Bottom) Participation ratio ϖ for the P (blue), NP (green), and full (brown) problems in one $L = 168$ ($N = 45\,395$) configuration.

This representation brings out three frequency domains defined as follows:

I. the $\omega < \omega_g$ domain, below the NP gap, where only P modes are present;
II. the intermediate frequency range $\simeq [\omega_g, c_{\rm L}^{\rm Born} k_c]$, in which the P and NP spectra overlap, which we subdivide as $\mathrm{II}' \equiv [\omega_g, c_{\rm T}^{\rm Born} k_c]$, where P phonons of both polarizations are present, and $\mathrm{II}'' \equiv [c_{\rm T}^{\rm Born} k_c, c_{\rm L}^{\rm Born} k_c]$ where the P spectrum only contains longitudinal-like phonons; and
III. the upper frequency range $\omega \gtrsim c_{\rm L}^{\rm Born} k_c$ where only NP modes exist.

In domain III, the full and NP DOS's are nearly indistinguishable, showing that the hybridization effects are extremely small. In II'', these effects remain weak, since $\rho^{\rm P} + \rho^{\rm NP}$ remains rather close to $\rho^{\rm full}$. They become prevalent, however, in domains II' and I, i.e., below the frequency $c_{\rm T}^{\rm Born} k_c$ where transverse-like modes are present in the P spectrum. This, we think, manifests the pre-eminent influence of the coupling between transverse phonons and NP states in determining the structure of the full spectrum in a broad frequency range encompassing both the Boson peak and the acoustic domain. This observation is reminiscent of the previous suggestions by several authors[26–29] that the Boson peak excess vibrations are mainly of transverse character.

Beyond these remarks, the most striking observation afforded by this plot is that, for the selected k_c value, which corresponds to the previously identified optimal separation scale between large and short wavelengths, the Boson peak position is nearly coincident with the boundary between domains I and II', i.e., with the position of the low energy gap in the NP spectrum. This is unlikely to be fortuitous, since this boundary separates resonant and non-resonant P–NP coupling regimes.

Let us now turn to the question of the spatial structure of the modes and, in particular, of their degree of localization. For this purpose, we consider the participation ratio that, for any particle displacement field **u**, reads

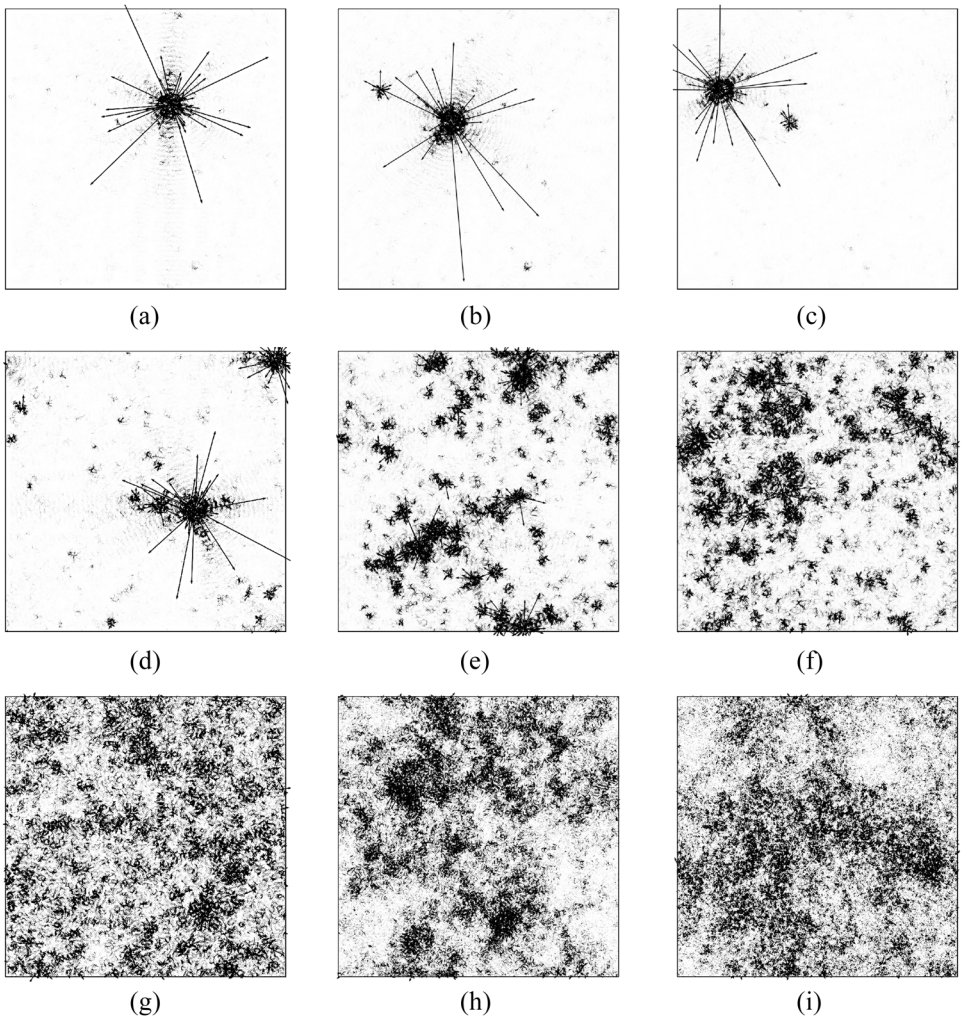

FIG. 7. A few NP modes for an $L = 168$ system and $k_c = 1.12$. (a) $n = 1$, $\overline{\omega} \simeq 1.53$, $\overline{\omega} \simeq 3 \times 10^{-4}$; (b) $n = 2$, $\omega \simeq 1.63$, $\overline{\omega} \simeq 3 \times 10^{-4}$; (c) $n = 3$, $\omega \simeq 1.65$, $\overline{\omega} \simeq 3 \times 10^{-4}$; (d) $n = 25$, $\omega \simeq 2$, $\overline{\omega} \simeq 6 \times 10^{-4}$; (e) $n = 132$, $\omega \simeq 2.5$, $\overline{\omega} \simeq 10^{-2}$; (f) $n = 456$, $\omega \simeq 3$, $\overline{\omega} \simeq 2 \times 10^{-2}$; (g) $n = 1719$, $\omega \simeq 4$, $\overline{\omega} \simeq 0.15$; (h) $n = 8939$, $\omega \simeq 7$, $\overline{\omega} \simeq 0.15$; and (i) $n = 25\,067$, $\omega \simeq 11$, $\overline{\omega} \simeq 0.2$.

$$\overline{\omega} = \frac{1}{N} \frac{\left(\sum_{i=1}^{N} \underline{u}_i^2\right)^2}{\sum_{i=1}^{N} \left(\underline{u}_i^2\right)^2}. \tag{21}$$

Since this quantity is equal to 1 for a homogeneous field and $1/N$ for a field localized on a single particle, it is often used to have some indication about the spatial extent of modes.[24,30–34] The participation ratios of the modes of the P, NP, and full problems, for one configuration of our $L = 168$ system, are displayed in Fig. 6, below the corresponding density of states.

This scatter plot clearly shows that the P modes (blue) are systematically extended, consistent with our previous conclusion that they are essentially plane waves.

Second, it reveals that the NP spectrum presents, close above ω_g, a non-negligible number of localized (small $\overline{\omega}$) modes: for instance, for the considered system, there are about 200 modes with $\overline{\omega} \leq 10^{-2}$. The spatial structure of the modes (labeled n, in the order of increasing ω), in different frequency domains, is illustrated in Fig. 7. As shown in Figs. 7(a)–7(c), the first few modes, close to the gap frequency, generally involve one or a very few centers. Note that modes 2 and 3 combine contributions from the same two centers, with different weights, which evidences hybridization effects, i.e., residual couplings within the NP problem. As long as $\overline{\omega} \lesssim 5 \times 10^{-2}$, the modes become increasingly multi-localized, i.e., can be viewed as involving hybridized centers, yet in a number that grows rapidly with the frequency, as shown in Figs. 7(d)–(f), corresponding to frequencies $\omega \simeq 2, 2.5, 3$. Beyond this [see Figs. 7(g)–7(i)], the contrast between large and small displacements is too small to discern any localization center.

We now turn to the modes of the full problem, which is defined by the recoupling between the P and NP sub-systems. As seen in the scatter plot (Fig. 5), like the P ones, the lowest frequency modes have $\overline{\omega}$ values $\simeq 1$. An example (mode $n = 5$, $\omega = 0.16$), displayed in Fig. 8(a), illustrates that these modes are essentially combinations of plane waves, with barely any visible hint for the presence of

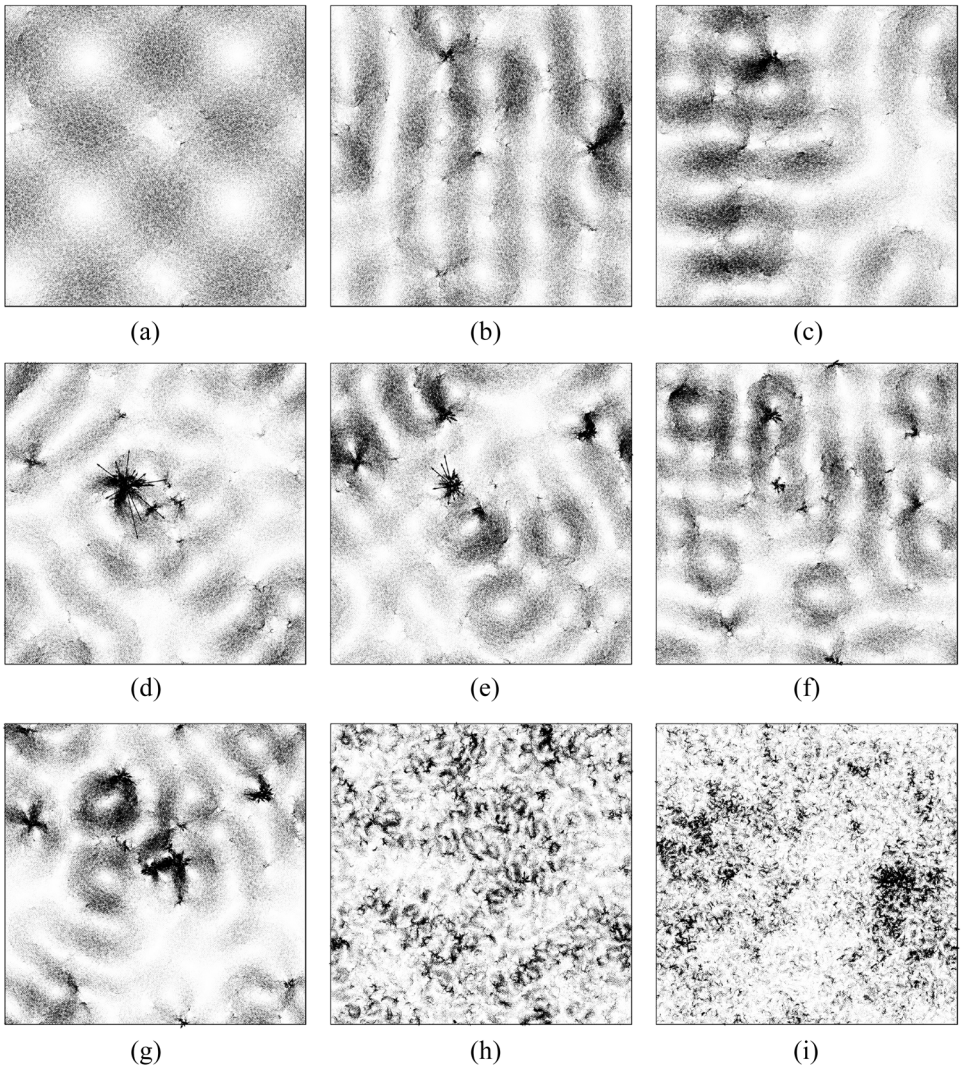

FIG. 8. A few modes of the full problem for the same $L = 168$ system as in Fig. 7. (a) $n = 5$, $\omega \simeq 0.16$, $\overline{\omega} \simeq 0.8$; (b) $n = 30$, $\omega \simeq 0.35$, $\overline{\omega} \simeq 0.48$; (c) $n = 31$, $\omega \simeq 0.35$, $\overline{\omega} \simeq 0.38$; (d) $n = 41$, $\omega \simeq 0.4$, $\overline{\omega} \simeq 3 \times 10^{-3}$; (e) $n = 53$, $\omega \simeq 0.43$, $\overline{\omega} \simeq 3.5 \times 10^{-2}$; (f) $n = 58$, $\omega \simeq 0.46$, $\overline{\omega} \simeq 0.36$; (g) $n = 59$, $\omega \simeq 0.46$, $\overline{\omega} \simeq 0.12$; (h) $n = 1271$, $\omega \simeq 2$, $\overline{\omega} \simeq 0.26$; and (i) $n = 4842$, $\omega \simeq 4$, $\overline{\omega} \simeq 0.16$.

non-affine contributions. Such contributions must, of course, exist since the plane-wave-like lowest modes of both the full and P problems with equal k's have different eigenfrequencies ($\simeq c_{\mathrm{T,L}}\, k$, with $c_{\mathrm{T,L}}^{\mathrm{full}} < c_{\mathrm{T,L}}^{\mathrm{Born}}$).

As the frequency increases across region I, the participation ratios of the full problem modes rapidly decay, and for $\omega \gtrsim 1$, they lie below about 0.3, a level that is clearly smaller than all $\overline{\omega}$ values for P modes. As shown in Figs. 8(b)–8(g), the modes in this frequency range show clear signs of mixing between the P plane-wave-like states, and localized oscillators, which correspond to the centers previously identified in the localized NP states.

As already emphasized by many authors,[24,30–34] in this lower part of the spectrum, some modes present very small $\overline{\omega}$ values. Here, the most localized one [Fig. 8(d), $\overline{\omega} \simeq 3 \times 10^{-3}$, $\omega \simeq 0.4$] is clearly dominated by a single center, which is the dominant one in mode $n = 2$ ($\overline{\omega} \simeq 3 \times 10^{-4}$, $\omega \simeq 1.63$), of the NP problem [Fig. 7(b)]. This specific case, where quasi-plane wave P states hybridize predominantly with a single NP local oscillator, permits us to identify the downward frequency shift of the oscillator, which turns out to be huge: dressing by the extended states reduces the oscillator frequency by a factor of about 4.

For the configuration examined here, there is only one such single-centered state. At least six centers can be identified in mode $n = 53$ [Fig. 8(e), $\overline{\omega} \simeq 3.5 \times 10^{-2}$, $\omega \simeq 0.43$], which is the next most localized one in region I. More generally, most of the states of the full problem in region I incorporate contributions from several centers: see, for example, Figs. 8(b), 8(c), 8(f), and 8(g). Additionally, neither the number nor the locations of the contributing centers show any clear correlation, when comparing consecutive states in the order of increasing frequencies [compare Figs. 8(b) and 8(c) and Figs. 8(f) and 8(g)].

Toward the upper end of region I and into region II, it becomes increasingly difficult to identify any localization center [see Fig. 8(h)]. The modes become increasingly complex and diffuse with a further increase in frequency [Fig. 8(i)].

The above analysis of modes in region I has brought to light several clear indications of a quite strong coupling between acoustic phonons and the NP localized oscillators: the magnitude of the identified frequency shift, the generic presence of several centers in the full problem modes, and the very small number of localized states in the full problem. As a consequence, there is no straightforward relation between the features of the rare localized states of the full problem, such as number, morphology (degree of localization, multiplicity of soft centers), or frequency, and those of the NP modes. Hence, contrary to an idea put forward by some authors (see Refs. 35 and 36 and references therein), the full problem localized modes cannot be interpreted as being the soft localized oscillators of defect theories.[1]

V. REINTRODUCING THE PHONON–NON-PHONON COUPLING

A. The scattering equation in the acoustic domain

Sound propagation in the considered material can be fully characterized by studying the response of the system to an imposed initial plane wave velocity field $\boldsymbol{\varphi}_{\underline{k},\underline{a}}$.[10,24] Since we focus on the acoustic domain ($k \ll k_c$), the initial perturbation is restricted to the P subspace so that the scattering problem decomposes into the coupled equations [see Eq. (13)]

$$\ddot{\mathbf{u}}^{\mathrm{p}} = -\boldsymbol{\mathcal{H}}^{\mathrm{p,p}}\mathbf{u}^{\mathrm{p}} - \boldsymbol{\mathcal{H}}^{\mathrm{p,np}}\mathbf{u}^{\mathrm{np}} + \delta(t)\,\boldsymbol{\varphi}_{\underline{k},\underline{a}}, \tag{22a}$$

$$\ddot{\mathbf{u}}^{\mathrm{np}} = -\boldsymbol{\mathcal{H}}^{\mathrm{np,p}}\mathbf{u}^{\mathrm{p}} - \boldsymbol{\mathcal{H}}^{\mathrm{np,np}}\mathbf{u}^{\mathrm{np}} \tag{22b}$$

with $\dot{\mathbf{u}}^{\mathrm{p}}(t) = \mathbf{u}^{\mathrm{p}}(t) = \mathbf{0}$ and $\dot{\mathbf{u}}^{\mathrm{np}}(t) = \mathbf{u}^{\mathrm{np}}(t) = \mathbf{0}$ for all $t < 0$. In the frequency representation, the above equation reads

$$(\omega + i\eta)^2\,\mathbf{u}^{\mathrm{p}} = \boldsymbol{\mathcal{H}}^{\mathrm{p,p}}\mathbf{u}^{\mathrm{p}} + \boldsymbol{\mathcal{H}}^{\mathrm{p,np}}\mathbf{u}^{\mathrm{np}} - \boldsymbol{\varphi}_{\underline{k},\underline{a}}, \tag{23a}$$

$$(\omega + i\eta)^2\,\mathbf{u}^{\mathrm{np}} = \boldsymbol{\mathcal{H}}^{\mathrm{np,p}}\mathbf{u}^{\mathrm{p}} + \boldsymbol{\mathcal{H}}^{\mathrm{np,np}}\mathbf{u}^{\mathrm{np}}, \tag{23b}$$

with $\eta > 0$ a small parameter. Eliminating $\mathbf{u}^{\mathrm{np}}$, one finds

$$(\omega + i\eta)^2\,\mathbf{u}^{\mathrm{p}} = \boldsymbol{\mathcal{H}}^{\mathrm{p,p}}\mathbf{u}^{\mathrm{p}} - \boldsymbol{\mathcal{Q}}(\omega)\mathbf{u}^{\mathrm{p}} - \boldsymbol{\varphi}_{\underline{k},\underline{a}} \tag{24}$$

with

$$\boldsymbol{\mathcal{Q}}(\omega) = \boldsymbol{\mathcal{H}}^{\mathrm{p,np}}\left[-(\omega + i\eta)^2 + \boldsymbol{\mathcal{H}}^{\mathrm{np,np}}\right]^{-1}\boldsymbol{\mathcal{H}}^{\mathrm{np,p}}. \tag{25}$$

Equation (24) is the full problem scattering equation, yet expressed as an equation of motion for the phonon part $\mathbf{u}^{\mathrm{p}}$ of the full displacement field. We see that the scattering amplitude is the sum of two contributions: the first, $\boldsymbol{\mathcal{H}}^{\mathrm{p,p}}$, directly couples phonons and governs scattering within the isolated P subspace [see Eq. (15)]; and the second, $\boldsymbol{\mathcal{Q}}(\omega)$, describes the indirect phonon–phonon coupling mediated by propagation within the isolated NP subspace. Due to the elimination of the NP degrees of freedom, $\boldsymbol{\mathcal{Q}}(\omega)$ is necessarily ω-dependent, i.e., time-retarded, and *a priori* non-local.

In order to eventually understand how the continuum limit is achieved, we need to rewrite Eq. (24) without an explicit reference to $\mathbf{u}^{\mathrm{p}}$, which is configuration-dependent, but instead in terms of the weights of the plane waves generating the P subspace, that is, using the coefficients $\widehat{\mathbf{u}}$ [see Eqs. (6) and (7)]. Left-multiplying Eq. (24) by $\left(\boldsymbol{\Phi}^{\dagger}\boldsymbol{\Phi}\right)^{-1}\boldsymbol{\Phi}^{\dagger}$ and using Eqs. (10) and (11), we obtain the full problem wave equation in terms of $\widehat{\mathbf{u}}$,

$$(\omega + i\eta)^2\,\boldsymbol{\Phi}^{\dagger}\boldsymbol{\Phi}\widehat{\mathbf{u}} = \boldsymbol{\Phi}^{\dagger}\boldsymbol{\mathcal{H}}\boldsymbol{\Phi}\widehat{\mathbf{u}} - \boldsymbol{\Phi}^{\dagger}\boldsymbol{\mathcal{Q}}(\omega)\boldsymbol{\Phi}\widehat{\mathbf{u}} - \boldsymbol{\Phi}^{\dagger}\boldsymbol{\Phi}\widehat{\boldsymbol{\varphi}}_{\underline{k},\underline{a}}. \tag{26}$$

Here, $\widehat{\boldsymbol{\varphi}}_{\underline{k},\underline{a}}$ is the component vector for the incoming plane wave $\boldsymbol{\varphi}_{\underline{k},\underline{a}}$: all its $(\underline{k}',\underline{a}')$ coefficients are equal to zero, except for the $(\underline{k}',\underline{a}') = (\underline{k},\underline{a})$ one, which is equal to 1.

Let us emphasize that Eq. (26) is the full discrete wave equation, but written in terms of plane wave coefficients. In this representation, the operator $\boldsymbol{\Phi}^{\dagger}\boldsymbol{\mathcal{H}}\boldsymbol{\Phi}$ corresponds to $\boldsymbol{\mathcal{H}}^{\mathrm{p,p}}$, which is the restriction of the Hessian to the P subspace; meanwhile, $\boldsymbol{\Phi}^{\dagger}\boldsymbol{\mathcal{Q}}(\omega)\boldsymbol{\Phi}$ accounts for the indirect coupling between P waves due to the small scale non-affinity. The projection formalism has thus enabled us to subsume all small scale non-affine effects to the presence, in Eq. (26), of a term involving the indirect effective scattering potential $\boldsymbol{\Phi}^{\dagger}\boldsymbol{\mathcal{Q}}(\omega)\boldsymbol{\Phi}$.

The solution of Eq. (26) is of the form

$$\widehat{\mathbf{u}} = \widehat{\mathcal{G}}\widehat{\boldsymbol{\varphi}}_{\underline{k},\underline{a}}, \tag{27}$$

with the Green function

$$\widehat{\mathcal{G}} = \left[-(\omega + i\eta)^2 \boldsymbol{\Phi}^\dagger\boldsymbol{\Phi} + \boldsymbol{\Phi}^\dagger\boldsymbol{\mathcal{H}}\boldsymbol{\Phi} - \boldsymbol{\Phi}^\dagger\boldsymbol{\mathcal{Q}}(\omega)\boldsymbol{\Phi}\right]^{-1}\boldsymbol{\Phi}^\dagger\boldsymbol{\Phi}. \tag{28}$$

Since the coefficient vector $\widehat{\boldsymbol{\varphi}}_{\underline{k},\underline{a}}$ is configuration-independent, the ensemble-averaged response can now be expressed as

$$\langle\widehat{\mathbf{u}}\rangle = \langle\widehat{\mathcal{G}}\rangle\widehat{\boldsymbol{\varphi}}_{\underline{k},\underline{a}}. \tag{29}$$

The average Green function $\langle\widehat{\mathcal{G}}\rangle$ accounts for the acoustic response of our glass.

Let us recall that the central objective underlying the construction of the projection formalism is to attempt to represent, in the long wavelength limit, an amorphous solid as an elastic continuum. A first step toward this goal was achieved when writing Eq. (26): we have then reduced the full problem to an equation of motion for a vector ($\widehat{\mathbf{u}}$) restricted to the P subspace. The ensuing question is whether, when taking the long-wavelength approximation of this equation, we obtain a Navier-like equation, i.e., a continuum problem featuring spatially fluctuating elastic constants.

From this perspective, it is useful to bear in mind that the discrete wave problem is written in terms of displacements from a mechanically equilibrated reference state and hence is most naturally compared with the Lagrangian form of continuum elasticity. In this latter representation, the fully tensorial wave equation for a spatially fluctuating elastic continuum reads

$$\ddot{\underline{\widehat{u}}}(\underline{k}) = -\int \mathrm{d}\underline{k}'\underline{\underline{\mathcal{D}}}(\underline{k},\underline{k}')\cdot\underline{\widehat{u}}(\underline{k}'), \tag{30}$$

where the kernel $\mathcal{D}^{\alpha\kappa}(\underline{k},\underline{k}')$ is of the form

$$\mathcal{D}^{\alpha\kappa}(\underline{k},\underline{k}') = \frac{1}{\rho V}k^\beta k'^\chi\,\widehat{\mathcal{S}}^{\alpha\beta\kappa\chi}(\underline{k}-\underline{k}'), \tag{31}$$

with $\rho = Nm/V$ being the mean density, V being the volume, and $\widehat{\mathcal{S}}_{\alpha\beta\kappa\chi}$ being the Fourier transform of the local elasticity tensor.

Explicitly introducing the polarizations of the vector field $\widehat{u}$ amounts to writing

$$\underline{\widehat{u}}(\underline{k}) = \sum_{\underline{a}\in\mathrm{pol.}(\underline{k})}\widehat{u}_{\underline{a}}(\underline{k})\,\underline{a} \tag{32}$$

with the sum running over the polarization vectors ($\{\underline{k}/k, \underline{k}^\perp/k\}$ in our 2D setting). In terms of $\widehat{u}_{\underline{a}}(\underline{k})$, the wave equation reads

$$\ddot{\widehat{u}}_{\underline{a}}(\underline{k}) = -\int \mathrm{d}\underline{k}'\sum_{\underline{a}'\in\mathrm{pol.}(\underline{k}')}\underline{\underline{\mathcal{D}}}_{\underline{a},\underline{a}'}(\underline{k},\underline{k}')\cdot\widehat{u}_{\underline{a}'}(\underline{k}') \tag{33}$$

with the linear kernel

$$\begin{aligned}\mathcal{D}_{\underline{a},\underline{a}'}(\underline{k},\underline{k}') &\equiv \underline{a}\cdot\mathcal{D}(\underline{k},\underline{k}')\cdot\underline{a}'\\ &= \frac{1}{\rho V}a^\alpha k^\beta a'^\kappa k'^\chi\widehat{\mathcal{S}}^{\alpha\beta\kappa\chi}(\underline{k}-\underline{k}').\end{aligned} \tag{34}$$

In Refs. 10 and 23, we showed that, to the lowest order in a long wavelength expansion, the coefficients of the Hessian are precisely of the above form, where the field $\widehat{\mathcal{S}}^{\alpha\beta\kappa\chi}$ can be explicitly written in terms of the interaction potential and particle positions.

The FE studied in Ref. 23 is the continuum problem (30) based on these elasticity coefficients. By construction, this approximation only accounts for the long wavelength form of $\boldsymbol{\Phi}^\dagger\boldsymbol{\mathcal{H}}\boldsymbol{\Phi}$. It, therefore, constitutes a lowest order approximation for the wave equation in the uncoupled P space, which is why, as discussed in Sec. III, it captures reasonably well the sound properties of the P problem, rather than those of the full one. Meanwhile, it completely overlooks the indirect coupling $\boldsymbol{\Phi}^\dagger\boldsymbol{\mathcal{Q}}(\omega)\boldsymbol{\Phi}$ and hence all small scale non-affine contributions.

B. Explicit form of the scattering equation for a pairwise pair potential

In order to go beyond the FE approximation, we need to explicit the form of the various terms in Eq. (26).

1. Mass factor

The coefficients of the "mass factor" $\boldsymbol{\Phi}^\dagger\boldsymbol{\Phi}$ read

$$\boldsymbol{\varphi}^\dagger_{\underline{k},\underline{a}}\boldsymbol{\varphi}_{\underline{k}',\underline{a}'} = \frac{\underline{a}\cdot\underline{a}'}{N}\sum_i e^{-i(\underline{k}-\underline{k}')\cdot\underline{r}_i}. \tag{35}$$

Note that, for $\underline{k}' = \underline{k}$, $\boldsymbol{\varphi}^\dagger_{\underline{k},\underline{a}}\boldsymbol{\varphi}_{\underline{k},\underline{a}'} = \underline{a}\cdot\underline{a}'$, while the average of the square norm $\langle|\boldsymbol{\varphi}^\dagger_{\underline{k},\underline{a}}\boldsymbol{\varphi}_{\underline{k}',\underline{a}'}|^2\rangle = \frac{(\underline{a}\cdot\underline{a}')^2}{N}S(\underline{k}-\underline{k}')$, with S being the structure factor.

2. Direct elasticity tensor

For a pairwise potential, the total force field $-\boldsymbol{\mathcal{H}}\boldsymbol{\varphi}_{\underline{k},\underline{a}}$ generated by a plane wave displacement reads

$$\left(-\boldsymbol{\mathcal{H}}\boldsymbol{\varphi}_{\underline{k},\underline{a}}\right)_i = -\frac{1}{\sqrt{N}}\sum_{j\neq i}\underline{\underline{M}}_{ij}\cdot\underline{a}\left(e^{i\underline{k}\cdot\underline{r}_j} - e^{i\underline{k}\cdot\underline{r}_i}\right), \tag{36}$$

where, for each pair (i,j),

$$M^{\alpha\kappa}_{ij} = \left(U''_{ij}(r_{ij}) - \frac{U'_{ij}(r_{ij})}{r_{ij}}\right)n^\alpha_{ij}n^\kappa_{ij} + \frac{U'_{ij}(r_{ij})}{r_{ij}}\,\delta^{\alpha\kappa}, \tag{37}$$

with $U(r)$ being the pair potential, $\underline{r}_{ij} = \underline{r}_j - \underline{r}_i$, and $\underline{n}_{ij} = \underline{r}_{ij}/r_{ij}$. The direct coupling term, therefore, is of the form

$$\boldsymbol{\varphi}^\dagger_{\underline{k},\underline{a}}\boldsymbol{\mathcal{H}}\boldsymbol{\varphi}_{\underline{k}',\underline{a}'} = \frac{1}{N}\sum_i\sum_{j>i}\underline{a}\cdot\underline{\underline{M}}_{ij}\cdot\underline{a}'\left(e^{-i\underline{k}\cdot\underline{r}_j} - e^{-i\underline{k}\cdot\underline{r}_i}\right)\left(e^{i\underline{k}'\cdot\underline{r}_j} - e^{i\underline{k}'\cdot\underline{r}_i}\right), \tag{38}$$

which can easily be recast as

$$\boldsymbol{\varphi}^\dagger_{\underline{k},\underline{a}}\boldsymbol{\mathcal{H}}\boldsymbol{\varphi}_{\underline{k}',\underline{a}'} = \frac{1}{\rho V}a^\alpha k^\beta a'^\kappa k'^\chi\,\widehat{\mathcal{S}}^{\alpha\beta\kappa\chi}(\underline{k},\underline{k}'), \tag{39}$$

with

$$\widehat{\mathcal{S}}^{\alpha\beta\kappa\chi}(\underline{k},\underline{k}') = \sum_i \sum_{j>i} M_{ij}^{\alpha\kappa} r_{ij}^{\beta} r_{ij}^{\chi}\, j_0\left(\frac{\underline{k}\cdot\underline{r}_{ij}}{2}\right) j_0\left(\frac{\underline{k}'\cdot\underline{r}_{ij}}{2}\right) e^{-i(\underline{k}-\underline{k}')\cdot\bar{\underline{r}}_{ij}}, \quad (40)$$

where $j_0(x) = \sin(x)/x$ and $\bar{\underline{r}}_{ij} = (\underline{r}_i + \underline{r}_j)/2$.

In view of Eq. (39), $\widehat{\mathcal{S}}^{\alpha\beta\kappa\chi}(\underline{k},\underline{k}')$ can be considered as a *generalized elasticity tensor*. Yet, since it depends on both $\underline{k}+\underline{k}'$ and $\underline{k}-\underline{k}'$ and not just on $\underline{k}-\underline{k}'$, its real space form is *a priori non-local*.

3. Indirect elasticity tensor

We now seek to analyze the indirect effective potential

$$\widehat{\boldsymbol{\mathcal{Q}}}(\omega) \equiv \boldsymbol{\Phi}^{\dagger}\boldsymbol{\mathcal{Q}}(\omega)\boldsymbol{\Phi} = \boldsymbol{\Phi}^{\dagger}\boldsymbol{\mathcal{H}}^{\mathrm{p,np}}\boldsymbol{\mathcal{G}}^{\mathrm{np,np}}(\omega)\boldsymbol{\mathcal{H}}^{\mathrm{np,p}}\boldsymbol{\Phi}, \quad (41)$$

where

$$\boldsymbol{\mathcal{G}}^{\mathrm{np,np}}(\omega) \equiv \left[-(\omega+i\eta)^2 + \boldsymbol{\mathcal{H}}^{\mathrm{np,np}}\right]^{-1} \quad (42)$$

is the Green function of the uncoupled NP subspace. We will first derive an explicit microscopic expression for $\widehat{\boldsymbol{\mathcal{Q}}}(\omega)$ in the case of pairwise interactions; then, we will calculate its asymptotic form in the low frequency, acoustic limit.

To proceed, we denote $\boldsymbol{\psi}_n$ as the nth NP eigenmode and ω_n^2 as its eigenvalue. This permits us to write the projector onto the NP space as

$$\mathbf{1} - \boldsymbol{\mathcal{P}} = \sum_n \boldsymbol{\psi}_n\, \boldsymbol{\psi}_n^{\dagger}, \quad (43)$$

where the sum runs over the $(N-M)d$ modes. Meanwhile, the NP Green function reads

$$\boldsymbol{\mathcal{G}}^{\mathrm{np,np}}(\omega) = \sum_n \frac{\boldsymbol{\psi}_n\, \boldsymbol{\psi}_n^{\dagger}}{\omega_n^2 - (\omega+i\eta)^2}. \quad (44)$$

We now write explicitly the components of the effective scattering potential,

$$\begin{aligned}\widehat{\mathcal{Q}}_{\underline{k},\underline{a},\underline{k}',\underline{a}'}(\omega) &= \boldsymbol{\varphi}_{\underline{k},\underline{a}}^{\dagger}\,\boldsymbol{\mathcal{Q}}(\omega)\,\boldsymbol{\varphi}_{\underline{k}',\underline{a}'} \\ &= \boldsymbol{\varphi}_{\underline{k},\underline{a}}^{\dagger}\boldsymbol{\mathcal{H}}(1-\boldsymbol{\mathcal{P}})\boldsymbol{\mathcal{G}}^{\mathrm{np,np}}(\omega)(1-\boldsymbol{\mathcal{P}})\boldsymbol{\mathcal{H}}\boldsymbol{\varphi}_{\underline{k}',\underline{a}'}, \end{aligned} \quad (45)$$

and noting that $(1-\boldsymbol{\mathcal{P}})\boldsymbol{\psi}_n = \boldsymbol{\psi}_n$, we find

$$\widehat{\mathcal{Q}}_{\underline{k},\underline{a},\underline{k}',\underline{a}'}(\omega) = \sum_n \frac{\left(\boldsymbol{\varphi}_{\underline{k},\underline{a}}^{\dagger}\boldsymbol{\mathcal{H}}\boldsymbol{\psi}_n\right)\left(\boldsymbol{\psi}_n^{\dagger}\boldsymbol{\mathcal{H}}\boldsymbol{\varphi}_{\underline{k}',\underline{a}'}\right)}{\omega_n^2 - (\omega+i\eta)^2}, \quad (46)$$

which brings forward the scalar products between the NP eigenvectors and the total force fields, such as $-\boldsymbol{\mathcal{H}}\boldsymbol{\varphi}_{\underline{k},\underline{a}}$, generated by the plane wave displacements. For pairwise potentials, these latter fields read explicitly,

$$\left(-\boldsymbol{\mathcal{H}}\boldsymbol{\varphi}_{\underline{k},\underline{a}}\right)_i = -\frac{1}{\sqrt{N}}\sum_{j\neq i}\underline{\underline{M}}_{ij}\cdot\underline{a}\left(e^{i\underline{k}\cdot\underline{r}_j} - e^{i\underline{k}\cdot\underline{r}_i}\right). \quad (47)$$

The NP components of these force fields are now calculated as follows:

$$\begin{aligned}-\boldsymbol{\varphi}_{\underline{k},\underline{a}}^{\dagger}\boldsymbol{\mathcal{H}}\boldsymbol{\psi}_n &= -\frac{1}{\sqrt{N}}\sum_i\sum_{j\neq i}\underline{a}\cdot\underline{\underline{M}}_{ij}\cdot\underline{\psi}_{n\,i}\left(e^{-i\underline{k}\cdot\underline{r}_j} - e^{-i\underline{k}\cdot\underline{r}_i}\right) \\ &= -\frac{1}{\sqrt{N}}\sum_{i<j}\underline{a}\cdot\underline{\underline{M}}_{ij}\cdot\left(\underline{\psi}_{n\,i} - \underline{\psi}_{n\,j}\right)\left(e^{-i\underline{k}\cdot\underline{r}_j} - e^{-i\underline{k}\cdot\underline{r}_i}\right) \\ &= -\frac{i}{\sqrt{N}}a^{\alpha}k^{\beta}\sum_{i<j}M_{ij}^{\alpha\kappa}\left(\psi_{n\,i}^{\kappa} - \psi_{n\,j}^{\kappa}\right)r_{ij}^{\beta}\,\frac{e^{-i\underline{k}\cdot\underline{r}_j} - e^{-i\underline{k}\cdot\underline{r}_i}}{i\underline{k}\cdot\underline{r}_{ij}} \\ &\equiv \frac{i}{\sqrt{N}}a^{\alpha}k^{\beta}\zeta_{n\,\underline{k}}^{\alpha\beta}. \end{aligned} \quad (48)$$

Here, the second order tensor

$$\zeta_{n\,\underline{k}}^{\alpha\beta} \equiv \sum_{i<j}M_{ij}^{\alpha\kappa}\left(\psi_{n\,i}^{\kappa} - \psi_{n\,j}^{\kappa}\right)r_{ij}^{\beta}\,\frac{e^{-i\underline{k}\cdot\underline{r}_i} - e^{-i\underline{k}\cdot\underline{r}_j}}{i\underline{k}\cdot\underline{r}_{ij}} \quad (49)$$

is the stress induced in P by the normalized displacement field $\boldsymbol{\psi}_n$.

In terms of these fields, the indirect scattering potential finally reads

$$\widehat{\mathcal{Q}}_{\underline{k},\underline{a},\underline{k}',\underline{a}'}(\omega) = \frac{1}{\rho V}a^{\alpha}k^{\beta}a'^{\kappa}k'^{\chi}\,\widehat{\mathcal{Z}}^{\alpha\beta\kappa\chi}(\omega,\underline{k},\underline{k}') \quad (50)$$

with $\rho = N/V$ and

$$\widehat{\mathcal{Z}}^{\alpha\beta\kappa\chi}(\omega,\underline{k},\underline{k}') \equiv \sum_n \frac{\zeta_{n\,\underline{k}}^{\alpha\beta}\,\zeta_{n\,\underline{k}'}^{\kappa\chi\,*}}{\omega_n^2 - (\omega+i\eta)^2}. \quad (51)$$

The above two equations show that, like $\boldsymbol{\Phi}^{\dagger}\boldsymbol{\mathcal{H}}\boldsymbol{\Phi}$, the indirect coupling $\boldsymbol{\Phi}^{\dagger}\boldsymbol{\mathcal{Q}}(\omega)\boldsymbol{\Phi}$ that, in Eq. (26), encapsulates all small scale non-affinity effects has the structure [Eq. (34)] of a fluctuating elasticity kernel. The associated $\widehat{\mathcal{Z}}^{\alpha\beta\kappa\chi}(\omega,\underline{k},\underline{k}')$ thus appears to be a *generalized elasticity tensor*, which, like $\widehat{\mathcal{S}}^{\alpha\beta\kappa\chi}(\underline{k},\underline{k}')$, is *non-local*, but also *retarted*.

C. Non-locality scale of the indirect elasticity tensor

The question then is to try and assess how the non-local and retardation effects contained in both $\widehat{\mathcal{S}}^{\alpha\beta\kappa\chi}(\underline{k},\underline{k}')$ and $\widehat{\mathcal{Z}}^{\alpha\beta\kappa\chi}(\omega,\underline{k},\underline{k}')$ show up in the long wavelength limit.

The FE approximation as derived in Refs. 10 and 23 was obtained by approximating the j_0 factors in Eq. (40) by the lowest order term of their small $\underline{k}$, $\underline{k}'$ expansions: $j_0(x) \simeq 1$. Higher orders in this expansion bring $\mathcal{O}(\underline{k}^2, \underline{k}'^2)$ terms, which suggests that non-local effects may show up as second gradient corrections to elasticity. It is only as long as these corrections remain negligible that $\boldsymbol{\Phi}^{\dagger}\boldsymbol{\mathcal{H}}\boldsymbol{\Phi}$ can be well approximated by usual elasticity and the P subspace by a Debye-like continuum. Therefore, the optimal (upper) k_c value of order 1 we previously identified empirically should be consistent with the relative amplitude of these non-local corrections remaining quite small. We will check this in Sec. VI A.

Let us now turn to the indirect elasticity tensor. For this purpose, it is important to recall that the NP spectrum presents a finite low frequency gap, which entails that the projection introduces a characteristic frequency scale, $\omega_g \simeq 1.5k_c$ (Sec. IV). Since we are specifically interested in the acoustic limit, we restrict our attention

to frequencies ω lying much below the gap frequency ω_g. We can thus drop the infinitesimal parameter $i\eta$ in Eq. (51). We choose from now on $k_c = 1.12$, which lies in the optimal range of P–NP separation (Sec. III) for which $\omega_g \simeq 1.7$.

We show in Appendix E that $\widehat{\mathcal{Z}}^{\alpha\beta\kappa\chi}$ can be written in terms of the Green function $\underline{\underline{\Gamma}}_l^{(ij)}(\omega)$ that governs the NP response to a force dipole $\pm\underline{f}$ applied on pair (i, j),

$$\underline{u}_l^{\rm np}(\omega) \equiv \underline{\underline{\Gamma}}_l^{(ij)}(\omega)\cdot\underline{f}. \tag{52}$$

Specifically, we find

$$\widehat{\mathcal{Z}}^{\alpha\beta\kappa\chi}(\omega,\underline{k},\underline{k}') = \sum_{l<m}\sum_{i<j}\mathcal{M}^{\alpha\kappa}_{ijlm}(\omega)\, r^{\beta}_{lm}\, r^{\chi}_{ij}\, j_0\left(\frac{\underline{k}\cdot\underline{r}_{lm}}{2}\right) \times j_0\left(\frac{\underline{k}'\cdot\underline{r}_{ij}}{2}\right) e^{i\underline{k}'\cdot\bar{\underline{r}}_{ij} - i\underline{k}\cdot\bar{\underline{r}}_{lm}} \tag{53}$$

with

$$\underline{\underline{\mathcal{M}}}_{ijlm}(\omega) = \underline{\underline{M}}_{lm}\cdot\left(\underline{\underline{\Gamma}}_l^{(ij)}(\omega) - \underline{\underline{\Gamma}}_m^{(ij)}(\omega)\right)\cdot\underline{\underline{M}}_{ij}. \tag{54}$$

Expression (53) shows that non-local corrections to $\widehat{\mathcal{Z}}^{\alpha\beta\kappa\chi}$ may arise from the j_0 factors (as for $\widehat{\mathcal{S}}^{\alpha\beta\kappa\chi}$) but also from the frequency-dependent pair–pair coupling introduced by $\mathcal{M}^{\alpha\kappa}_{ijlm}(\omega)$. The degree of locality of $\mathcal{Z}^{\alpha\beta\kappa\chi}$, therefore, also depends on that of $\underline{\underline{\Gamma}}_l^{(ij)}$.

We display in Fig. 9 the static response $\Gamma_l^{(ij)}(\omega = 0)\cdot\underline{f}$ to dipoles located on two different pairs taken from the configuration used in Fig. 7 and for both longitudinal and transverse (to the pair direction) orientations of the source dipole. The first pair [Figs. 9(a) and 9(b)] is chosen in the core of the lowest NP eigenmode, which is highly localized [see Fig. 7(a)]. The second one [Figs. 9(c) and 9(d)] is taken at an arbitrary point away from this core. These pictures show that independently of the location and orientation of the excitation, the response is highly localized.

In order to quantify this statement, we have systematically computed the normalized response for all pair sources in $L = 84$ systems. Figure 10 shows the pair-, configuration-, and angle-averaged square norm of this field as a function of the distance r from the source pair midpoint. At intermediate distances, i.e., up to $2\pi/k_c$, it exhibits an exponential decay with an extremely short characteristic length $\ell \simeq 0.8$. Beyond $2\pi/k_c$, where its amplitude is already minute, it crosses over to a osc./r^3 asymptotic decay, which is expected due to the sharp cutoff at k_c.

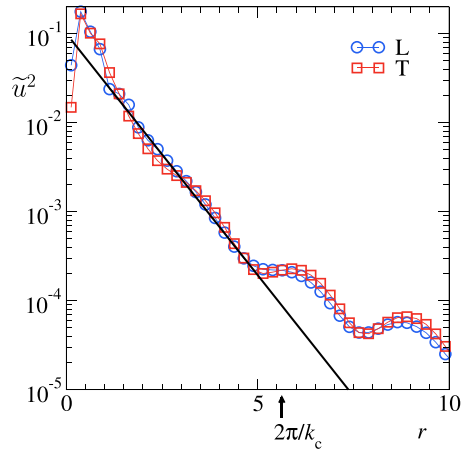

FIG. 10. The square amplitude $\widetilde{u}^2$ of the normalized displacement field $\Gamma_l^{(ij)}(\omega = 0)\cdot\underline{f}$ [Eq. (52)] vs the distance r to the source pair midpoint, after pair- and angle-averaging, for both longitudinal (L) and transverse (T) orientations of the source dipoles relative to the pair orientations. The line is a fit $\propto\exp(-r/\ell)$ with $\ell = 0.8$.

The rapid decay of $\Gamma_l^{(ij)}(\omega)$ with $\|\underline{r}_l - \bar{\underline{r}}_{ij}\|$ entails a comparable one for $\underline{\underline{\mathcal{M}}}_{ijlm}$ with $\|\bar{\underline{r}}_{ij} - \bar{\underline{r}}_{lm}\|$. In Eq. (53), recasting $i\underline{k}'\cdot\bar{\underline{r}}_{ij} - i\underline{k}\cdot\bar{\underline{r}}_{lm} = i(\underline{k}' - \underline{k})\cdot(\bar{\underline{r}}_{ij} + \bar{\underline{r}}_{lm})/2 + i(\underline{k}' + \underline{k})\cdot(\bar{\underline{r}}_{ij} - \bar{\underline{r}}_{lm})/2$, since $\|\bar{\underline{r}}_{ij} - \bar{\underline{r}}_{lm}\| \lesssim 1$ and $k, k' < k_c$, we see that it is legitimate to expand the exponential factor up to the second order in powers of $i(\underline{k}' + \underline{k})\cdot(\bar{\underline{r}}_{ij} - \bar{\underline{r}}_{lm})/2$. The pair–pair coupling introduced by $\mathcal{M}^{\alpha\kappa}_{ijlm}(\omega)$ therefore brings $\mathcal{O}[(\underline{k} + \underline{k}')^2]$ non-local contributions in addition to those arising from the expansion of the j_0 factors. It should hence also generate a second gradient correction, a form we will now see explicitly emerging from a detailed analysis of the average indirect elasticity tensor.

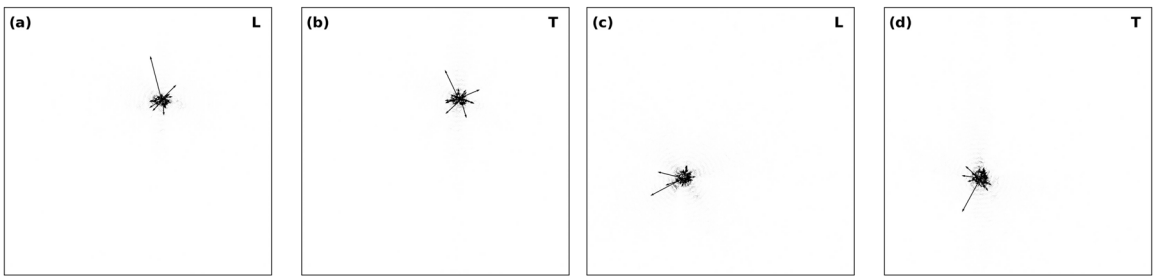

FIG. 9. In the configuration of Fig. 7: the response, normalized so that the largest arrows are of comparable sizes, to force dipoles. [(a) and (b)] The dipole is applied to a pair located inside the core of the lowest NP eigenmode [Fig. 7(a)]. [(c) and (d)] The dipole is applied to an arbitrary pair, far away from this core. The forces are colinear with the pair orientation on (a) and (c); they are tranverse to the pair orientation on (b) and (d).

VI. AVERAGE ELASTICITY TENSORS AND SOUND SPEED ESTIMATES

In real space, the direct and indirect elasticity tensors are two-point functions: $\mathcal{S}^{\alpha\beta\kappa\chi}(\underline{r},\underline{r}')$ and $\mathcal{Z}^{\alpha\beta\kappa\chi}(\omega,\underline{r},\underline{r}')$. Thanks to the translation invariance, their ensemble averages only depend on $\underline{r}-\underline{r}'$ and therefore provide information on their degree of non-locality. In Fourier space, these averages are diagonal in $\underline{k}$,

$$\begin{aligned}\langle\widehat{\mathcal{S}}^{\alpha\beta\kappa\chi}(\underline{k},\underline{k}')\rangle &= \langle\widehat{\mathcal{S}}^{\alpha\beta\kappa\chi}(\underline{k},\underline{k})\rangle\,\delta_{\underline{k},\underline{k}'},\\ \langle\widehat{\mathcal{Z}}^{\alpha\beta\kappa\chi}(\omega,\underline{k},\underline{k}')\rangle &= \langle\widehat{\mathcal{Z}}^{\alpha\beta\kappa\chi}(\omega,\underline{k},\underline{k})\rangle\,\delta_{\underline{k},\underline{k}'}.\end{aligned} \tag{55}$$

To analyze such rank-4 tensor fields, we use the formalism of Refs. 23 and 37 and decompose rank-2 tensors on the radial basis in Fourier space,

$$\begin{aligned}\underline{\underline{T}}^{\hat{\underline{k}}}_{1} &= \frac{1}{\sqrt{2}}\left(\hat{\underline{k}}\,\hat{\underline{k}}+\hat{\underline{\vartheta}}\,\hat{\underline{\vartheta}}\right),\\ \underline{\underline{T}}^{\hat{\underline{k}}}_{2} &= \frac{1}{\sqrt{2}}\left(\hat{\underline{k}}\,\hat{\underline{k}}-\hat{\underline{\vartheta}}\,\hat{\underline{\vartheta}}\right),\\ \underline{\underline{T}}^{\hat{\underline{k}}}_{3} &= \frac{1}{\sqrt{2}}\left(\hat{\underline{k}}\,\hat{\underline{\vartheta}}+\hat{\underline{\vartheta}}\,\hat{\underline{k}}\right),\\ \underline{\underline{T}}^{\hat{\underline{k}}}_{4} &= \frac{1}{\sqrt{2}}\left(\hat{\underline{k}}\,\hat{\underline{\vartheta}}-\hat{\underline{\vartheta}}\,\hat{\underline{k}}\right).\end{aligned} \tag{56}$$

In terms of stress, the first element of this basis corresponds to pressure, the next two to the two orientations of pure shear stresses, and the last one to the stress asymmetry, i.e., the torque density.

Using this formalism, a rank-2 tensor $\underline{\underline{\sigma}}$ is represented by a four-component vector denoted as $\underset{\sim}{\sigma}^{\hat{\underline{k}}}$ and a rank-4 tensor field $\widehat{\mathcal{A}}^{\alpha\beta\kappa\chi}(\underline{k})$ by a field of 4×4 matrices denoted as $\mathring{\underline{\underline{\underline{\underline{\mathcal{A}}}}}}(\underline{k})=\{\mathring{\mathcal{A}}^{ab}(\underline{k}),a,b=1,\ldots,4\}$, where the mark $^\circ$ signals that the above radial tensor basis is used at any $\underline{k}$.[37]

In order to obtain $\mathring{\mathcal{S}}^{ab}$, as detailed in Appendix B, one must first compute the matrix representation of $\widehat{\mathcal{S}}^{\alpha\beta\kappa\chi}$ in the tensor basis analogous to that of Eq. (56), yet based on the Cartesian vectors, before performing a Cartesian-to-radial matrix transform.[23,37]

The average of the indirect elasticity tensor in the radial matrix form, $\mathring{\mathcal{Z}}^{ab}$, is obtained using

$$\langle\mathring{\mathcal{Z}}^{ab}(\omega,\underline{k},\underline{k})\rangle = \left\langle\sum_n \frac{\zeta^{\hat{\underline{k}}}_{n\underline{k}\,a}\,\zeta^{\hat{\underline{k}}\,*}_{n\underline{k}\,b}}{\omega_n^2-(\omega+i\eta)^2}\right\rangle, \tag{57}$$

which involves the vector components $\underset{\sim}{\zeta}^{\hat{\underline{k}}}_{n\underline{k}}=\{\zeta^{\hat{\underline{k}}}_{n\underline{k}\,a}\}$, where $a=1,\ldots,4$ of the rank-2 tensor $\underline{\underline{\zeta}}_{n\underline{k}}$.

To compare the k-space values of these elasticity tensors for different system sizes, it is necessary to normalize them by the system volume. We thus introduce

$$\begin{aligned}\underset{\approx}{\mathfrak{s}}(\underline{k}) &\equiv \frac{1}{V}\langle\mathring{\underline{\underline{\underline{\underline{\mathcal{S}}}}}}(\underline{k},\underline{k})\rangle,\\ \underset{\approx}{\mathfrak{z}}(\omega,\underline{k}) &\equiv \frac{1}{V}\langle\mathring{\underline{\underline{\underline{\underline{\mathcal{Z}}}}}}(\omega,\underline{k},\underline{k})\rangle.\end{aligned} \tag{58}$$

A. Average direct elasticity tensor

Thanks to global inversion symmetry, the $\underset{\approx}{\mathfrak{s}}$ matrix, which is real-valued, is also symmetric. Moreover, material isotropy entails that it is independent of the orientation of vector $\underline{k}$ and is of the form[23]

$$\underset{\approx}{\mathfrak{s}}(\underline{k}) = \underset{\approx}{\mathfrak{s}}(k) = \begin{pmatrix}\mathfrak{s}_{11} & \mathfrak{s}_{12} & 0 & 0\\ \mathfrak{s}_{12} & \mathfrak{s}_{22} & 0 & 0\\ 0 & 0 & \mathfrak{s}_{33} & \mathfrak{s}_{34}\\ 0 & 0 & \mathfrak{s}_{34} & \mathfrak{s}_{44}\end{pmatrix}. \tag{59}$$

Its non-zero components, as computed in $L=84$ systems, are displayed in Fig. 11 (there is no observable difference with the same data in $L=168$ systems). Note that at $\underline{k}=\underline{0}$, $\langle\mathring{\underline{\underline{\underline{\underline{\mathcal{S}}}}}}(\underline{k},\underline{k})\rangle$ [Eq. (40)] reduces to the Born elasticity tensor,[38] which is diagonal in the following matrix representation:[23]

$$\frac{1}{V}\mathring{\underline{\underline{\underline{\underline{\mathcal{S}}}}}}^{\text{Born}} = \begin{pmatrix}2K^{\text{B}}-p & 0 & 0 & 0\\ 0 & 2\mu^{\text{B}}-p & 0 & 0\\ 0 & 0 & 2\mu^{\text{B}}-p & 0\\ 0 & 0 & 0 & -p\end{pmatrix}\delta_{\underline{k},\underline{0}}, \tag{60}$$

with p being the pressure and K^{B} and μ^{B} being the bulk and shear moduli, respectively—which for 2D Born elasticity verifies that $K^{\text{B}}=2\mu^{\text{B}}$.[38] In the $k\to0$ limit, hence, the off-diagonal components of $\underset{\approx}{\mathfrak{s}}(\underline{k})$, $\mathfrak{s}_{12}$, and $\mathfrak{s}_{34}$ vanish, while the diagonal ones converge to finite values.

We see that all components of $\underset{\approx}{\mathfrak{s}}$ are only very weakly k-dependent on the relevant $[0,k_c]$ range, with the overall variations of the diagonal ones being at most of order 4%. Consistently, the diagonal (respectively, off-diagonal) components are very well fitted by quadratic (respectively, quartic) expressions with characteristic k values that share a common order of magnitude $k^*\simeq5$. We show

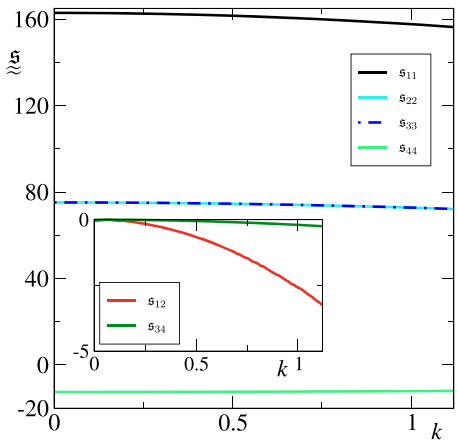

FIG. 11. Non-zero elements of $\underset{\approx}{\mathfrak{s}}(k)$ [Eq. (59)] vs k, for $k<k_c=1.12$, as measured in $L=84$ systems. (Inset) A zoomed-in view of the off-diagonal components, $\mathfrak{s}_{12}$ and $\mathfrak{s}_{34}$.

in Appendix B that these characteristic k values are structural properties expressible analytically as pair averages of combinations of r_{ij}, U'_{ij}, and U'_{ij}.

Non-locality corrections to direct elasticity are thus of relative order $(k_c/5)^2$, which justifies directly our choice of a k_c value of order 1.

B. Average indirect elasticity tensor

We have restricted our attention to ω values that lie much below the gap $\omega_g \simeq 1.7$ (for $k_c = 1.12$) of the NP spectrum. This guarantees that, like $\underset{\approx}{\mathfrak{E}}$, $\underset{\approx}{\mathfrak{z}}$ is real-valued. It is hence also symmetric and of the same block-diagonal form as in Eq. (59). Moreover, in the low-frequency acoustic domain, we may expand it in powers of ω^2,

$$\underset{\approx}{\mathfrak{z}}(\omega,k) = \underset{\approx}{\mathfrak{z}}^{(0)}(k) + \omega^2 \underset{\approx}{\mathfrak{z}}^{(1)}(k) + \mathcal{O}(\omega^4), \tag{61}$$

and only retain the first two terms.

The non-zero components of $\underset{\approx}{\mathfrak{z}}^{(0)}(k)$ and $\underset{\approx}{\mathfrak{z}}^{(1)}(k)$, as computed in $L = 84$ systems, are plotted in Figs. 12 and 13, respectively. We have checked that these data are indistinguishable from those obtained with $L = 168$. These figures show that both $\underset{\approx}{\mathfrak{z}}^{(0)}(k)$ and $\underset{\approx}{\mathfrak{z}}^{(1)}(k)$ exhibit similar structures, which are described as follows.

First, for both $i = 0$ and 1, $\mathfrak{z}^{(i)}_{22}$ and $\mathfrak{z}^{(i)}_{33}$ are nearly identical, systematically larger than the other $\mathfrak{z}^{(i)}_{ab}$, and have a finite $k \to 0$ limit.

Second, all four other fields vanish in the $k \to 0$ limit, which can be understood as follows.

We show in Appendix C that the fourth stress component $\zeta^{\hat{k}}_{n\underline{k}\,4}$, which is present due to the *local* breaking of rotational invariance, vanishes when $k = 0$ due to the condition of mechanical equilibrium that is the defining property of any reference inherent state. This reflects the invariance of the average medium under *global* rotations.

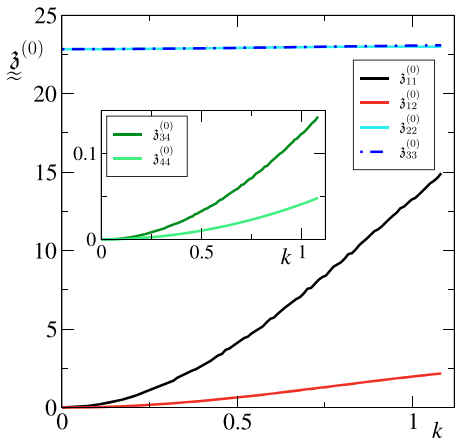

FIG. 12. Non-zero elements of $\underset{\approx}{\mathfrak{z}}^{(0)}(k)$ [Eq. (61)] vs k, for $k < k_c = 1.12$, as measured in $L = 84$ systems. (Inset) A zoomed-in view of the small components, $\mathfrak{z}^{(0)}_{34}$ and $\mathfrak{z}^{(0)}_{44}$.

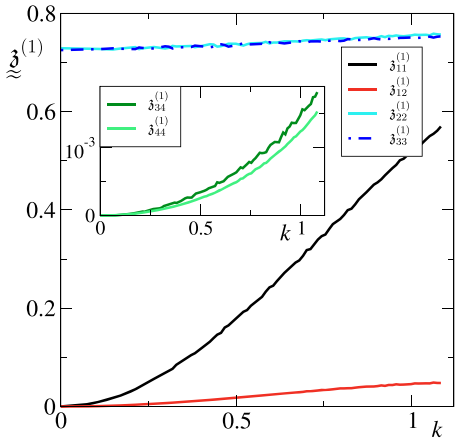

FIG. 13. Non-zero elements of $\underset{\approx}{\mathfrak{z}}^{(1)}(k)$ [Eq. (61)] vs k, for $k < k_c = 1.12$, as measured in $L = 84$ systems. (Inset) A zoomed-in view of the small components, $\mathfrak{z}^{(1)}_{34}$ and $\mathfrak{z}^{(1)}_{44}$.

It entails that, at any frequency, both $\mathfrak{z}_{34}(\omega,k)$ and $\mathfrak{z}_{44}(\omega,k)$ vanish in the $k \to 0$ limit.

Besides, for a power-law repulsive pair potential, such as used here, $\zeta^{\hat{k}}_{n\underline{k}\,1}$ and $\zeta^{\hat{k}}_{n\underline{k}\,4}$ are proportional, a relation that is also nearly verified by Lennard-Jones glasses and Roskilde systems.[39] In such a case, the pressure component $\zeta^{\hat{k}}_{n\underline{k}\,1}$ and hence $\mathfrak{z}_{11}(\omega,k)$ and $\mathfrak{z}_{12}(\omega,k)$ also vanish for $k = 0$.

Third and finally, all the curves of Figs. 12 and 13 are essentially indistinguishable from their fits (not shown) by the analytical expression $C_0 - C_1\, e^{-k^2\ell^2/2}$, where $C_0 = C_1$, except for $\mathfrak{z}^{(i)}_{22}$ and $\mathfrak{z}^{(i)}_{33}$. Moreover, the associated lengths (ℓ) range typically between 0.5 and 1.5, comparable with the estimate previously obtained by inspection of the NP response to pair dipoles, and entails that the average elasticity tensor $\langle \mathcal{Z}^{\alpha\beta\kappa\chi}(\omega, \underline{r}_0, \underline{r}_0 + \underline{r})\rangle$ is highly local.

It follows from the above that the constant and k^2 terms suffice to fit $\underset{\approx}{\mathfrak{z}}^{(0)}(k)$ and $\underset{\approx}{\mathfrak{z}}^{(1)}(k)$ up to $k \gtrsim 0.5$, i.e., much beyond the acoustic k-range. *The average indirect elasticity tensor then appears to assume the form of a frequency-dependent second gradient kernel.*[40]

C. Sound speed estimates

The most naive approximation we may construct for the exact wave equation (26) consists in replacing the operators $\mathbf{\Phi}^\dagger\mathbf{\Phi}$, $\mathbf{\Phi}^\dagger\mathcal{H}\mathbf{\Phi}$, and $\mathbf{\Phi}^\dagger\mathcal{Q}(\omega)\mathbf{\Phi}$ by their ensemble averages. Since $\langle\mathbf{\Phi}^\dagger\mathbf{\Phi}\rangle$ is the identity matrix, we then obtain a generalized Navier equation for an effective continuum with the elasticity tensor, $\langle\underset{\approx}{\mathcal{S}}\rangle - \langle\underset{\approx}{\mathcal{Z}}\rangle$.

In view of Eqs. (50), (55), and (58), the average kernel $\langle\mathbf{\Phi}^\dagger\mathcal{Q}(\omega)\mathbf{\Phi}\rangle$ is diagonal in both wavevector and polarization so that its coefficients can be split into the longitudinal and transverse ones,

$$\langle \widehat{Q}^{\mathrm{LL}}_{\underline{k},\underline{k}}(\omega)\rangle \equiv \langle \widehat{Q}_{\underline{k},\hat{\underline{k}},\underline{k},\hat{\underline{k}}}(\omega)\rangle = \frac{k^2}{\rho}\,\mathfrak{z}_{\mathrm{LL}}(\omega,k),$$
$$\langle \widehat{Q}^{\mathrm{TT}}_{\underline{k},\underline{k}}(\omega)\rangle \equiv \langle \widehat{Q}_{\underline{k},\hat{\underline{\vartheta}},\underline{k},\hat{\underline{\vartheta}}}(\omega)\rangle = \frac{k^2}{\rho}\,\mathfrak{z}_{\mathrm{TT}}(\omega,k), \tag{62}$$

with

$$\mathfrak{z}_{\mathrm{LL}} \equiv \frac{1}{2}(\mathfrak{z}_{11}+\mathfrak{z}_{12}+\mathfrak{z}_{21}+\mathfrak{z}_{22}),$$
$$\mathfrak{z}_{\mathrm{TT}} \equiv \frac{1}{2}(\mathfrak{z}_{33}-\mathfrak{z}_{34}-\mathfrak{z}_{43}+\mathfrak{z}_{44}). \tag{63}$$

The average direct elasticity kernel $\langle \mathbf{\Phi}^\dagger \boldsymbol{\mathcal{H}} \mathbf{\Phi}\rangle$ is also diagonal and exhibits exactly the same form with $\mathfrak{z}$ replaced by $\mathfrak{s}$.

Within this approximation, and using the second order expansion [Eq. (61)] for $\underset{\approx}{\mathfrak{z}}(\omega,k)$, the acoustic dispersion relations read

$$\omega^2 = \frac{k^2}{\rho}\left(\mathfrak{s}_{\mathrm{pp}} - \mathfrak{z}^{(0)}_{\mathrm{pp}}\right) - \omega^2\frac{k^2}{\rho}\,\mathfrak{z}^{(1)}_{\mathrm{pp}} \tag{64}$$

with p = L,T, and thus, the sound speeds are estimated as

$$\left(c^{\mathrm{eff}}_{\mathrm{p}}\right)^2 = \frac{1}{\rho}\,\frac{\mathfrak{s}_{\mathrm{pp}} - \mathfrak{z}^{(0)}_{\mathrm{pp}}}{1+\frac{k^2}{\rho}\,\mathfrak{z}^{(1)}_{\mathrm{pp}}}. \tag{65}$$

As we saw above, the coefficients of $\underset{\approx}{\mathfrak{s}}$, $\underset{\approx}{\mathfrak{z}}^{(0)}$, and $\underset{\approx}{\mathfrak{z}}^{(1)}$ are well approximated, in the whole P domain, by quadratic functions of k. The curvatures are negative for the coefficients of $\underset{\approx}{\mathfrak{s}}$ and negative for those of $\underset{\approx}{\mathfrak{z}}^{(0)}$ and $\underset{\approx}{\mathfrak{z}}^{(1)}$. It follows that the above sound speeds are both of the form $c^{\mathrm{eff}}_{\mathrm{p}} \simeq c^{\mathrm{eff}\,(0)}_{\mathrm{p}} + c^{\mathrm{eff}\,(1)}_{\mathrm{p}}\,k^2$, with $c^{\mathrm{eff}\,(1)}_{\mathrm{p}} < 0$. The average medium approximation therefore predicts that, in the large wavelength limit, sound speeds decrease with increasing k. This k-dependence is a signature of non-local and retarded effects.

In Table I, we compare the $k = 0$ sound speed values in this approximation (third column) with the Born approximation and the P (Sec. III) and full problem values. For both the longitudinal and transverse sound speeds, the average medium approximation we constructed above is seen to account for 70% of the mismatch between the full problem and the Born approximation. This is to be compared with the 4% correction obtained when solving propagation in the uncoupled P subspace. Therefore, this approximation, although quite rough, confirms that non-affinity effects result overwhelmingly from the coupling with the NP subspace.

TABLE I. Long-wavelength limit of sound speeds for various approximations and for the full problem.

	Born	P problem	Average medium	Full
$c_{\mathrm{L}}(k=0)$	8.6	8.58	8.2	8.04
$c_{\mathrm{T}}(k=0)$	4.41	4.37	3.53	3.17

D. Origin of non-affine corrections to the average elasticity tensor

The question naturally arises of whether the above indirect elastic correction originates primarily from the highly localized NP modes, akin to soft zones that lie close above the gap ω_g (see Sec. IV). For this purpose, we consider $\underset{\approx}{\mathfrak{z}}(\omega,k|\Omega)$, the contribution to $\underset{\approx}{\mathfrak{z}}(\omega,k)$ arising only from the NP modes of frequencies $\omega_n < \Omega$,

$$\underset{\approx}{\mathfrak{z}}(\omega,k|\Omega) = \frac{1}{V}\left\langle \sum_{\omega_n<\Omega} \frac{\underline{\zeta}^{\hat{\underline{k}}}_{n\underline{k}}\,\underline{\zeta}^{\hat{\underline{k}}\,*}_{n\underline{k}}}{\omega_n^2-\omega^2}\right\rangle. \tag{66}$$

We restrict our attention to its value for $\omega = k = 0$, since it is $\underset{\approx}{\mathfrak{z}}^{(0)}(\omega=0)$ which provides the main correction to the static elastic moduli. Only $\mathfrak{z}^{(0)}_{22}(0|\Omega)$ and $\mathfrak{z}^{(0)}_{33}(0|\Omega)$ are non-zero, and they are nearly indistinguishable. The former, displayed in Fig. 14, turns out to increase very regularly over the whole extent of the NP spectrum, clearly ruling out the idea that it would be controlled selectively by the few softer, localized modes. On the contrary, its very regular growth suggest that all modes, hence all scales smaller than k_c^{-1}, and all regions of space, contribute comparably.

This conclusion is further substantiated by the examination of $\underset{\approx}{\mathfrak{z}}$ in the time domain, which is computed as detailed in Appendix D. The two non-zero components of $\underset{\approx}{\mathfrak{z}}(t,k=0)$ are displayed in Fig. 15: they exhibit a very sharp peak at an unexpectedly small time $t^{\mathrm{peak}} \simeq 0.1$ (in LJ units). This peak is followed by a few, highly damped oscillations.

The interpretation of these features is straightforward. Let us recall indeed that $\underset{\approx}{\mathfrak{z}}(t)$ is determined by $\boldsymbol{\mathcal{Q}}(t) = \boldsymbol{\mathcal{H}}^{\mathrm{p,np}}\boldsymbol{\mathcal{G}}^{\mathrm{np,np}}(t)\boldsymbol{\mathcal{H}}^{\mathrm{np,p}}$ [Eq. (25)], which can be understood as the force generated, in P, at time t by the displacement $\boldsymbol{\mathcal{G}}^{\mathrm{np,np}}\boldsymbol{\mathcal{H}}^{\mathrm{np,p}}$, which is the NP response to the force impulse $\boldsymbol{\mathcal{H}}^{\mathrm{np,p}}$ applied at time $t = 0$. Following this impulse, each atom is kicked by a force impulse out of its equilibrium position and starts oscillating in its cage. The main peak of $\underset{\approx}{\mathfrak{z}}(t)$ corresponds to the time at which atoms reach

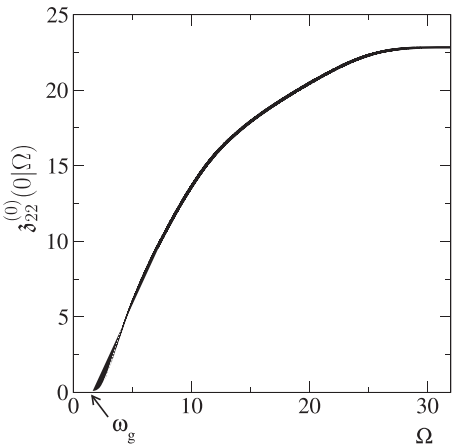

FIG. 14. Partial contribution to $\mathfrak{z}_{22}(\omega=0,k=0)$ arising from NP modes of frequencies $\omega_n < \Omega$ as a function of Ω.

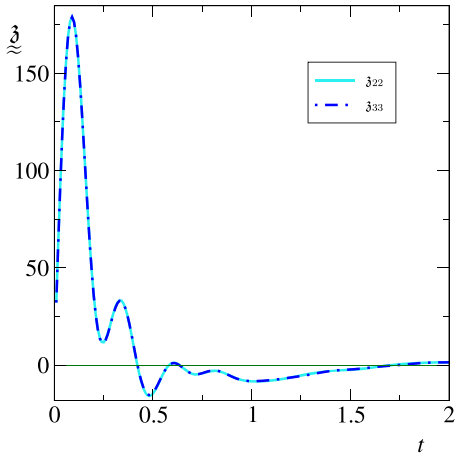

FIG. 15. Time evolution of the non-zero components of $\underset{\approx}{\vartheta}(t, k = 0)$ as averaged in $L = 84$ systems ($L = 168$ data are identical).

on average the maximum displacement within their cage. The very strong damping indicates that the back signal into the P space is washed out, after a fraction of an oscillation, by destructive interferences due to the local disorder. This further documents that the average NP response, hence the correction to macroscopic moduli, adds up rather democratically contributions from all atoms.

VII. SUMMARY AND DISCUSSION

In this work, we have shown that the projection formalism permits us to recast the microscopic, discrete equations governing sound propagation in an amorphous solid as an acoustic scattering problem in an elastic continuum.

This formalism relies on the introduction of a cutoff k_c that separates long and short wavelengths, which defines two associated subspaces, P and NP, respectively. The key observation that justifies the relevance of this separation is that the P spectrum remains quasi-linear (Debye-like) over the whole extent of its k domain ($k < k_c$), as long as k_c remains smaller than a rather large finite value $k_c^{\max}$ ($\simeq 1$), corresponding to a lengthscale ($\simeq 6$) of the order of a few interatomic distances only. Under this condition, the sound speeds are k_c-independent and equal to their Born values. We thus find that there exists a natural spatial scale $2\pi/k_c^{\max}$ of separation between long and short wavelengths such that, for $k_c = k_c^{\max}$, (i) the P subspace is a very weakly inhomogeneous elastic continuum, while (ii) the NP subspace concentrates all non-affine atomic motions, and (iii) P wave scattering is essentially due to the coupling with the NP subspace, the eigenstates of which play the role of dynamical scatterers.

The most striking feature of the NP spectrum is the presence of a low frequency gap, the existence of which can be understood as a necessary consequence of the P–NP separation. Indeed, reconstructing the full problem by recoupling the P and NP subspaces inevitably leads to hybridization-induced downward shifts of the eigenfrequencies of the low lying NP modes. The stability of the full problem demands the shifted eigenvalues to be positive, hence introduces constraints on the NP eigenvalues.

To illustrate how the full problem stability requirement constrains the gap value, let us consider a schematic problem in which one low NP eigenmode only, $\boldsymbol{\psi}^{\rm NP}$ of frequency $\omega^{\rm NP}$, is recoupled with the P problem. Approximating the P eigenstates by plane waves $\boldsymbol{\varphi}_{\underline{k},\underline{a}}$ of eigenfrequencies $\omega_{\underline{k},\underline{a}}$, the Hessian of the recoupled problem reads

$$\begin{pmatrix} \ddots & & 0 & \vdots \\ & \left(\omega_{\underline{k},\underline{a}}\right)^2 & & b_{\underline{k},\underline{a}} \\ 0 & & \ddots & \vdots \\ \cdots & b^*_{\underline{k},\underline{a}} & \cdots & \left(\omega^{\rm NP}\right)^2 \end{pmatrix}. \tag{67}$$

The upper left block is the P subspace, diagonal Hessian matrix; the coupling coefficients are $b_{\underline{k},\underline{a}} = \boldsymbol{\varphi}^\dagger_{\underline{k},\underline{a}} \boldsymbol{\mathcal{H}} \boldsymbol{\psi}^{\rm NP}$ calculated in Eq. (48).

Denoting $\mathbf{b} = \{b_{\underline{k},\underline{a}}\}$ as the associated column vector, the positive definiteness of the above matrix is equivalent to that of both the upper block $\mathbf{A}$ and its Schur complement $\left(\omega^{\rm NP}\right)^2 - \mathbf{b}^\dagger \mathbf{A}^{-1}\mathbf{b}$. The first condition holds by definition, and the second, since the Schur complement is a scalar, reduces to the following inequality:

$$\begin{aligned} \left(\omega^{\rm NP}\right)^2 > \mathbf{b}^\dagger \mathbf{A}^{-1}\mathbf{b} &= \sum_{\underline{k},\underline{a}} \frac{|b_{\underline{k},\underline{a}}|^2}{\left(\omega_{\underline{k},\underline{a}}\right)^2} \\ &\simeq \int_0^{c_{\rm L}k_c} {\rm d}\omega \, \frac{\omega}{2\pi\bar{\rho}} \left\langle \frac{N|b^{\rm L}(\omega)|^2}{\omega^2} \middle| \omega \right\rangle \\ &\quad + \int_0^{c_{\rm T}k_c} {\rm d}\omega \, \frac{\omega}{2\pi\bar{\rho}} \left\langle \frac{N|b^{\rm T}(\omega)|^2}{\omega^2} \middle| \omega \right\rangle, \end{aligned} \tag{68}$$

where we have considered that the P spectrum is the Debye one and with $\bar{\rho} = N/L^2$ being the mass density. Since [see Eq. (48)] $|b^{\rm L,T}(\omega)|^2 \sim k^2/N$, it follows that $\omega^{\rm NP} \gtrsim C\, k_c$, with C being a constant.

This argument shows that the stability of the full problem constrains ω_g to be finite and agrees with our observation (see the inset of Fig. 4) that ω_g scales as k_c, which supports that the NP spectrum extends as much as allowed by the stability requirement.

Besides we found that, when projection is implemented for the natural separation scale $2\pi/k_c^{\max}$, the gap turns out to lie close to the Boson peak frequency. Since we found $\omega_g \approx 2k_c$, it follows that $2\pi/k_c^{\max} \approx 4\pi/\omega^{\rm BP}$. This value is in remarkable agreement with the Boson peak lengthscale (see Refs. 20 and 21 and references therein), $2\pi c_{\rm T}/\omega^{\rm BP}$, with $c_{\rm T}$ (here ≈ 3.17) being the transverse sound speed, which was proposed to reflect the size of elastic heterogeneities and was recently found to match the core size of quasi-localized excitations.[22] What our paper achieves in this regard is to establish explicitly that the Boson peak lengthscale does separate a weakly dispersive elastic continuum from short range heterogeneities and thus constitutes a natural coarse-graining lengthscale for glasses.

The projection formalism allows us to reconsider the assumptions usually made in defect theories. Indeed, it shows that (i) the scattering dynamical "defects" are the eigenstates of the NP problem; (ii) their spectrum is bounded below by a finite gap, of the order of the Boson peak frequency: this directly contradicts the assumption made in defect theories that the spectrum of scatterers extends down to zero frequency.[1] Besides (iii), as discussed in Sec. IV, only a small fraction of the eigenstates are highly localized, and except for the lowest frequency ones, they are multi-centered.

These results lead us to caution against attempts to access the scatterers on the sole basis of the analysis of the localized eigenstates of the full problem. Within the projection formalism, the full problem eigenstates, indeed, emerge from the same recoupling mechanisms that produces scattering in the first place. They are not the cause of scattering, but just one of its consequences, hence provide direct information neither about the structure nor about the frequency of the scatterers.

As already mentioned, acoustic wave scattering is controlled by the indirect phonon–phonon coupling mediated by propagation within the NP subspace. This coupling, which acts within the P subspace, gives rise to an effective scattering potential that can be written explicitly in terms of the Hessian matrix of the microscopic problem. We are able to write explicitly the complete scattering operator $[\mathbf{\Phi}^\dagger \mathcal{H} \mathbf{\Phi} - \mathbf{\Phi}^\dagger \mathcal{Q}(\omega) \mathbf{\Phi}]$ as the sum of a direct and an indirect contributions. Note that this decomposition demonstrates that the effects of structural disorder cannot be expressed via the introduction of an additive, frequency-independent term in the full Hessian of an ordered system, as assumed in some phenomenological approaches.

The analysis of Eq. (26) then permits us to recast the wave equation for sound propagation in the full problem into a Navier-like continuum equation, yet with a generalized elasticity tensor that is not only retarded, since the scatterers are dynamical objects, but also non-local.

In order to evaluate the importance of non-locality effects, we have examined in detail the average generalized elasticity coefficients in the low frequency, acoustic range, where $\omega \ll \omega_g$. We found that the average elasticity coefficients, which define the mean effective medium, are quasi-local yet incorporate second gradient elasticity contributions associated with a small, but finite lengthscale, comparable with the interatomic distance. Estimating, on this basis, the first order corrections to the zeroth order Born sound speeds yields quite satisfactory results:

(i) In the $k \to 0$ limit, it accounts for $\simeq$70% of the mismatch between the full problem values and their Born approximations.
(ii) It correctly predicts, as resulting from both non-locality and retardation, the numerically observed downward curvatures of the $c_{L,T}(k)$ curves.[7,10]

The above results put us in a position to return to the important issue, central to fluctuating elasticity models,[2] whether or not, when dealing with acoustic scattering, it is legitimate to represent an amorphous solid by an inhomogeneous elastic continuum with *local and (implicitly) static* elastic moduli. Previous numerical efforts to access such local moduli[41–44] have proceeded by the inspection of the linear response of small regions isolated from the surrounding medium. This does permit us to define local moduli but leaves open the question of how to recouple their values into an elastic continuum compatible with the microscopic dynamics.

Here, we have been able to rigorously reduce the microscopic acoustic dynamics of the discrete solid to the wave equation for an inhomogeneous elastic continuum. However, this continuum is non-standard, its elasticity tensor being both *non-local and retarded*, two features that, as we saw, are responsible for the k-dependence of sound speeds. The question then naturally arises of the role played by these features in sound damping and of whether they can be neglected, as done in fluctuating elasticity models.

For this purpose, we first note that, in the acoustic domain, due to the low-frequency gap ω_g of the NP spectrum, it is legitimate to expand generalized elasticity coefficients in powers of the small parameter $(\omega/\omega_g)^2$. The lowest order, adiabatic approximation of this expansion amounts to assuming that the NP response is instantaneous, hence to setting the lhs's of Eqs. (22b) and (23b) to zero. Integrating Eq. (22) after this change permits us to completely neglect retardation effects while retaining the non-locality in full.

This adiabatic approximation amounts to replacing $Z(\omega; \underline{k}, \underline{k}')$ by its $\omega = 0$ expression. Under this assumption, non-local effects can then be eliminated by assuming $Z(0; \underline{k}, \underline{k}')$ to be independent of $\underline{k} + \underline{k}'$, i.e., to assume its value for $\underline{k} + \underline{k}' = 0$. Note that, in contrast with the elimination of retardation effects, this latter approximation does not result from a controlled expansion in a small parameter.

To test these two approximation schemes, we numerically integrate the resulting wave equations. These integrations being quite resource-intensive,[45] we are limited to use system sizes of at most $L = 168$. As a consequence, since size effects have been shown to arise for k about six times $2\pi/L$, the accessible k range is limited downwards to $k \gtrsim 0.2$. We compare in Fig. 16 the resulting damping coefficients with those of the full problem (black), which scale

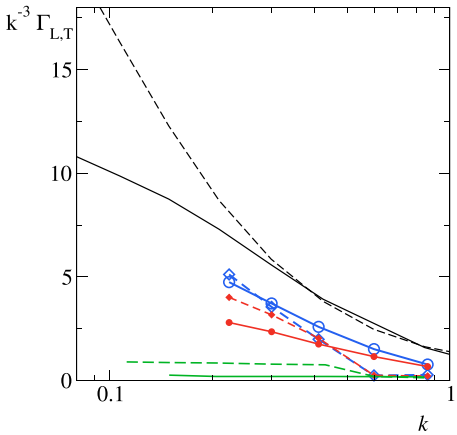

FIG. 16. Damping coefficients $\Gamma_{L,T}/k^3$ vs wavevector for longitudinal (dashed line with diamonds) and transverse (solid line with circles) waves in the full problem [black (from Ref. 10], in the uncoupled P problem (green), and in the adiabatic (blue) and local adiabatic (red) approximations (see the text).

as $\propto -k^3 \ln k$ in a low-k range down to $k \simeq 0.05$.[10] We also plot as a point of comparison the corresponding quantities for the uncoupled P problem. These data show that while non-affinity has a controlling influence on damping, the sole neglect of retardation (blue curves) yields $\Gamma_{L,T}$ values that are smaller by ≈30% but seem to track the full problem ones over the (limited) accessible k-range. In contrast, when both retardation and non-locality are neglected (red curves), the $\Gamma_{L,T}$ curves not only lie further away below the full problem data but are increasingly so as k decreases, suggesting the possibility of a different scaling, an issue that will, of course, demand being able to implement the above-defined approximations in much larger systems, a task out of the scope of the present work.

This latter observation shows that non-locality has a strong influence on sound propagation. This might appear paradoxical in view of the smallness of the associated lengthscale, of the order of an interatomic distance. However, it gains meaning when one notes that our formalism provides a controlled way to perform the program proposed by Barrat and co-workers[41,43,44] to split an amorphous solid into atomic patches. Recoupling the P and NP problems, i.e., the large and small scale dynamics, indeed amounts to patching up together "boxes" of size $\simeq 2\pi/k_c$. In real space, this would necessarily introduce a small length associated with the width of atomic boundaries binding these boxes together. On this basis, we surmise that the non-standard Rayleigh scaling of sound damping results from the compatibility conditions introduced by the re-embedding of each patch into its environment.

In conclusion, we have built here a framework that, using the projection formalism, permits us to rigorously separate an amorphous medium into an elastic continuum and a set of states that subsume the effects of small-scale structural disorder and act as dynamical scatterers for the phonons of the continuum. After validating in detail the relevance of this approach to a pairwise interaction system, we showed that the small scale disorder effects can be fully reduced to the existence, in the Navier-like wave equation of the continuum, of an indirect elasticity tensor that is both retarded and non-local. We have shown that both retardation and non-locality have non-negligible effects on sound speed dispersion and on the magnitude of sound attenuation. The question of the respective impacts of these two features on the large wavelength scaling of sound damping remains open and will be the subject of future investigations. Other issues of interest include (i) assessing how preparation history affects small-scale non-affinity and thus influences acoustic scattering and (ii) examining whether this description extends to systems such as covalent glasses.

ACKNOWLEDGMENTS

This work benefited from a French government grant managed by ANR within the framework of the National Program Investments for the Future (Grant No. ANR-11-LABX-0022-01).

APPENDIX A: NUMERICAL MODEL

Simulations are performed using the 2D binary soft sphere model of Ref. 10, which comprises large (L) and small (S) particles of equal masses $m = 1$, radii $R_L = 0.5$ and $R_S = 0.3$, in a number ratio $N_L/N_S \simeq (1+\sqrt{5})/4$. The simulation cell is square, periodic, of dimension $L \times L$, and the number density $\rho = N/L^2 = 1.6$. The potential is pairwise, with the contribution of any pair of atoms i and j being of the form

$$V_{ij}(r_{ij}) = 4\epsilon_{ij}\left(\frac{\sigma_{ij}}{r_{ij}}\right)^{12} + \alpha_{ij}\left(\frac{r_{ij}}{\sigma_{ij}}\right)^{4} + \beta_{ij}\left(\frac{r_{ij}}{\sigma_{ij}}\right)^{2} + \gamma_{ij}, \tag{A1}$$

if the interatomic distance $r_{ij} < r_{ij}^c \equiv 2\sigma_{ij}$, and $V_{ij}(r_{ij}) = 0$ otherwise. Here, $\sigma_{ij} \equiv R_i + R_j$, $\epsilon_{LL} = \epsilon_{SS} = 0.25$, and $\epsilon_{LS} = 0.17$, and the parameters α_{ij}, β_{ij}, and γ_{ij} are chosen so that V_{ij} vanishes at the second order at the interaction cutoff r_{ij}^c.

APPENDIX B: COMPUTATION OF THE AVERAGE DIRECT ELASTICITY TENSOR

From Eq. (40), we write

$$\mathcal{S}^{\alpha\beta\kappa\chi}(\underline{k},\underline{k}) = \sum_i \sum_{j>i} M_{ij}^{\alpha\kappa} r_{ij}^{\beta} r_{ij}^{\chi} \left[j_0\left(\frac{\underline{k}\cdot\underline{r}_{ij}}{2}\right)\right]^2 \tag{B1}$$

and single out the contribution of each pair,

$$\begin{aligned}\mathcal{S}_{ij}^{\alpha\beta\kappa\chi} &\equiv M_{ij}^{\alpha\kappa} r_{ij}^{\beta} r_{ij}^{\chi} \\ &= r_{ij}^2\, U_{ij}''\, n_{ij}^{\alpha} n_{ij}^{\beta} n_{ij}^{\kappa} n_{ij}^{\chi} + r_{ij}\, U_{ij}'\, t_{ij}^{\alpha} n_{ij}^{\beta} t_{ij}^{\kappa} n_{ij}^{\chi}\end{aligned} \tag{B2}$$

with $\underline{t}_{ij} = (-n_{ij}^y, n_{ij}^x)$. We need to write the above rank-4 tensor as a 4×4 matrix in the tensor basis of Eq. (56), yet based on the Cartesian vectors $\underline{e}_x, \underline{e}_y$. To do so, we first write the components of the tensors $\underline{n}\,\underline{n}$ and $\underline{t}\,\underline{n}$ in this basis

$$n_{ij}^{\alpha} n_{ij}^{\beta} = \frac{1}{\sqrt{2}} \begin{vmatrix} 1 \\ \cos 2\theta_{ij} \\ \sin 2\theta_{ij} \\ 0 \end{vmatrix} \qquad t_{ij}^{\alpha} n_{ij}^{\beta} = \frac{1}{\sqrt{2}} \begin{vmatrix} 0 \\ -\sin 2\theta_{ij} \\ \cos 2\theta_{ij} \\ -1 \end{vmatrix} \tag{B3}$$

from which we deduce the 4×4 matrix forms of the rank-4 tensors $\underline{\underline{\underline{\underline{A}}}} = \underline{n}\,\underline{n}\,\underline{n}\,\underline{n}$ and $\underline{\underline{\underline{\underline{B}}}} = \underline{t}\,\underline{n}\,\underline{t}\,\underline{n}$,

$$\underline{\underline{A}} = \frac{1}{2}\begin{pmatrix} 1 & \cos 2\theta_{ij} & \sin 2\theta_{ij} & 0 \\ \cos 2\theta_{ij} & \frac{1}{2}(1+\cos 4\theta_{ij}) & \frac{1}{2}\sin 4\theta_{ij} & 0 \\ \sin 2\theta_{ij} & \frac{1}{2}\sin 4\theta_{ij} & \frac{1}{2}(1-\cos 4\theta_{ij}) & 0 \\ 0 & 0 & 0 & 0 \end{pmatrix} \tag{B4}$$

and

$$\underline{\underline{B}} = \frac{1}{2}\begin{pmatrix} 0 & 0 & 0 & 0 \\ 0 & \frac{1}{2}(1-\cos 4\theta_{ij}) & -\frac{1}{2}\sin 4\theta_{ij} & \sin 2\theta_{ij} \\ 0 & -\frac{1}{2}\sin 4\theta_{ij} & \frac{1}{2}(1+\cos 4\theta_{ij}) & -\cos 2\theta_{ij} \\ 0 & \sin 2\theta_{ij} & -\cos 2\theta_{ij} & 1 \end{pmatrix}. \tag{B5}$$

The calculation of $\underline{\underline{\widehat{S}}}(\underline{k},\underline{k})$ then proceeds by considering, for each pair, the matrix $\underline{\underline{S}}_{ij} = r_{ij}^2\, U_{ij}''\, \underline{\underline{A}} + r_{ij}\, U_{ij}'\, \underline{\underline{B}}$ and then computing [see Eq. (B1)] each component of

$$\widehat{\underline{\underline{\underline{\underline{S}}}}}(\underline{k},\underline{k}) = \sum_i \sum_{j>i} \left(r_{ij}^2\, U_{ij}''\, \underline{\underline{\underline{\underline{A}}}} + r_{ij}\, U_{ij}'\, \underline{\underline{\underline{\underline{B}}}} \right) \left[j_0\left(\frac{\underline{k}\cdot\underline{r}_{ij}}{2} \right) \right]^2. \tag{B6}$$

This tensor field is then averaged over configurations and put in radial form, i.e., in the tensor basis [Eq. (56)], using the matrix transform[23,37]

$$\mathring{\underline{\underline{\underline{\underline{S}}}}}(\underline{k},\underline{k}) = \underline{\underline{\underline{\underline{R}}}}^{(2)}(\theta) \cdot \widehat{\underline{\underline{\underline{\underline{S}}}}}(\underline{k},\underline{k}) \cdot \underline{\underline{\underline{\underline{R}}}}^{(2)}(-\theta) \tag{B7}$$

with

$$\underline{\underline{\underline{\underline{R}}}}^{(2)}(\theta) = \begin{pmatrix} 1 & 0 & 0 & 0 \\ 0 & \cos 2\theta & \sin 2\theta & 0 \\ 0 & -\sin 2\theta & \cos 2\theta & 0 \\ 0 & 0 & 0 & 1 \end{pmatrix}. \tag{B8}$$

When ensemble-averaging the Cartesian form of $\widehat{\underline{\underline{\underline{\underline{S}}}}}(\underline{k},\underline{k})$, all contributions involving sines in tensors $\underline{\underline{\underline{\underline{A}}}}$ and $\underline{\underline{\underline{\underline{B}}}}$ vanish by symmetry. Besides, if we retain only the first two terms in the Taylor expansion of $j_0^2(x) = 1 - \frac{x^2}{3} + \mathcal{O}(k^4)$, all the contributions $\propto \cos 4\theta_{ij}$ also vanish. It follows that $\mathfrak{s}_{22} - \mathfrak{s}_{33} = \mathcal{O}(k^4)$, i.e., vanishes up to the second order.

Without loss of generality, we can take $\underline{k} = k\underline{e}_x$ to compute $\mathfrak{s}^{11}(\underline{k})$. At the second order in k, it yields

$$\begin{aligned} \mathfrak{s}^{11}(\underline{k}) &= \frac{1}{2V} \left\langle \sum_i \sum_{j>i} r_{ij}^2\, U_{ij}'' \left[j_0\left(\frac{\underline{k}\cdot\underline{r}_{ij}}{2} \right) \right]^2 \right\rangle \\ &\simeq \frac{1}{2V} \left\langle \sum_i \sum_{j>i} r_{ij}^2\, U_{ij}'' \right\rangle - \frac{k^2}{24V} \left\langle \sum_i \sum_{j>i} r_{ij}^2\, U_{ij}''\, (r_{ij}^x)^2 \right\rangle. \end{aligned} \tag{B9}$$

Thanks to isotropy, replacing $(r_{ij}^x)^2$ by $(r_{ij}^y)^2$ does not change the value of the last average. Hence, we can equivalently write

$$\mathfrak{s}^{11}(\underline{k}) \simeq \frac{1}{2V} \left\langle \sum_i \sum_{j>i} r_{ij}^2\, U_{ij}'' \right\rangle - \frac{k^2}{48V} \left\langle \sum_i \sum_{j>i} r_{ij}^4\, U_{ij}'' \right\rangle. \tag{B10}$$

Finally, $\mathfrak{s}^{11} \simeq C[1 - (k/k^*)^2 + \cdots]$ with the characteristic wavevector amplitude,

$$(k_{11}^*)^2 = 24\, \frac{\left\langle \sum_i \sum_{j>i} r_{ij}^2\, U_{ij}'' \right\rangle}{\left\langle \sum_i \sum_{j>i} r_{ij}^4\, U_{ij}'' \right\rangle}. \tag{B11}$$

We can perform the same calculation for $\mathfrak{s}^{22}$ and $\mathfrak{s}^{33}$ that, at second order, are identical and find

$$(k_{22}^*)^2 = (k_{33}^*)^2 = 24\, \frac{\left\langle \sum_i \sum_{j>i} r_{ij}^2\, U_{ij}'' + r_{ij}\, U_{ij}' \right\rangle}{\left\langle \sum_i \sum_{j>i} r_{ij}^4\, U_{ij}'' + r_{ij}^3\, U_{ij}' \right\rangle}, \tag{B12}$$

while for $\mathfrak{s}^{44}$,

$$(k_{44}^*)^2 = 24\, \frac{\left\langle \sum_i \sum_{j>i} r_{ij}\, U_{ij}' \right\rangle}{\left\langle \sum_i \sum_{j>i} r_{ij}^3\, U_{ij}' \right\rangle}. \tag{B13}$$

In the case of a power-law potential $U_{ij} \propto 1/r_{ij}^n$, these quantities are exactly equal to one another and reduce to $24\,\langle \sum_i \sum_{j>i} r_{ij}^{-n} \rangle / \langle \sum_i \sum_{j>i} r_{ij}^{2-n} \rangle$. For our system, we find the associated $k^* \simeq 5.5$.

APPENDIX C: VANISHING OF $\underline{\underline{\zeta}}_{n\underline{k}}$ COMPONENTS AT $k = 0$

The field $\underline{\underline{\zeta}}_{n\underline{k}}$ defined in Eq. (49) can be expressed as the scalar product

$$\zeta_{n\underline{k}}^{\alpha\beta} = \sum_i \psi_{ni}^{\kappa} \left(\Xi_{\underline{k}\,i}^{\alpha\beta\kappa} \right)^*, \tag{C1}$$

which is the nth NP component of the discrete rank-3 tensor field,

$$\Xi_{\underline{k}\,i}^{\alpha\beta\kappa} \equiv -\sum_j M_{ij}^{\alpha\kappa}\, r_{ij}^{\beta}\, \frac{e^{i\underline{k}\cdot\underline{r}_i} - e^{i\underline{k}\cdot\underline{r}_j}}{i\underline{k}\cdot\underline{r}_{ij}}. \tag{C2}$$

Let us split the indices of the above into the pair (α, β) and κ. Thus, for a given (α, β), $M_{ij}^{\alpha\kappa} r_{ij}^{\beta}$ can be viewed as the components of the vector $\underline{\underline{M}}_{ij} \cdot \underline{\underline{\epsilon}}^{(\alpha\beta)} \cdot \underline{r}_{ij}$, with $\epsilon_{\kappa\chi}^{(\alpha\beta)} = \delta_{\kappa\alpha}\, \delta_{\chi\beta}$ the unit strain of orientation (α, β). $\Xi_{\underline{k}\,i}^{\alpha\beta\kappa}$ then appears to be a force field associated with a strain of orientation $\underline{\underline{\epsilon}}^{(\alpha\beta)}$, which is modulated by a pair- and $\underline{k}$-dependent amplitude.

For each pair ij, using Eq. (37), we write explicitly

$$M_{ij}^{\alpha\kappa}\, r_{ij}^{\beta} = r_{ij}\, U_{ij}''\, n_{ij}^{\alpha}\, n_{ij}^{\beta}\, n_{ij}^{\kappa} + U_{ij}'\, t_{ij}^{\alpha}\, n_{ij}^{\beta}\, t_{ij}^{\kappa}. \tag{C3}$$

We now fix κ so that the above rank-3 tensors can be viewed as rank-2 tensors for the indices (α, β), which we may then write as a dimension-4 vector, in the tensor basis, analogous to Eq. (56), but based on the Cartesian basis vectors $\underline{e}_x, \underline{e}_y$. We thus obtain for $M_{ij}^{\alpha\kappa} r_{ij}^{\beta}$ the component vector,

$$M_{ij}^{\alpha\kappa}\, r_{ij}^{\beta} = \frac{1}{\sqrt{2}} \begin{vmatrix} r_{ij}\, U_{ij}''\, n_{ij}^{\kappa} \\ r_{ij}\, U_{ij}''\, n_{ij}^{\kappa} \cos 2\theta_{ij} - U_{ij}'\, t_{ij}^{\kappa} \sin 2\theta_{ij} \\ r_{ij}\, U_{ij}''\, n_{ij}^{\kappa} \sin 2\theta_{ij} + U_{ij}'\, t_{ij}^{\kappa} \cos 2\theta_{ij} \\ -U_{ij}'\, t_{ij}^{\kappa} \end{vmatrix}. \tag{C4}$$

It now appears that the fourth vector component (associated with indices $\alpha\beta$, for fixed κ) of $\Xi_{\underline{k}\,i}^{\alpha\beta\kappa}$ is

$$\Xi_{\underline{k}\,i}^{4\kappa} = \frac{1}{\sqrt{2}} \sum_j U_{ij}'\, t_{ij}^{\kappa}\, \frac{e^{i\underline{k}\cdot\underline{r}_i} - e^{i\underline{k}\cdot\underline{r}_j}}{i\underline{k}\cdot\underline{r}_{ij}}. \tag{C5}$$

For $k = 0$, this reduces to $\Xi_{\underline{0}\,i}^{4\kappa} = -\frac{1}{\sqrt{2}} \sum_j U_{ij}'\, t_{ij}^{\kappa} = -\frac{1}{\sqrt{2}} (-f_i^y, f_i^x)$ with

$$\underline{f}_i = \sum_j U_{ij}'\, \underline{n}_{ij} = \underline{0}, \tag{C6}$$

the resulting force on atom i in the reference inherent state. Mechanical balance therefore implies the $\underline{k} = \underline{0}$ value of $\Xi_{\underline{0}\,i}^{4\kappa} = 0$.

The first vector component of $\Xi_{\underline{k}\,i}^{\alpha\beta\kappa}$ is

$$\Xi_{\underline{k}\,i}^{1\kappa} = -\frac{1}{\sqrt{2}} \sum_j r_{ij} U''_{ij}\, n_{ij}^{\kappa} \frac{e^{i\underline{k}\cdot\underline{r}_i} - e^{i\underline{k}\cdot\underline{r}_j}}{i\underline{k}\cdot\underline{r}_{ij}}, \tag{C7}$$

which reduces to $\Xi_{\underline{0}\,i}^{1\kappa} = \frac{1}{\sqrt{2}} \sum_j r_{ij} U''_{ij}\, n_{ij}^{\kappa}$ when $k = 0$. For the power-law repulsive potential, since $U''_{ij} \propto U'_{ij}/r_{ij}$, up to a fixed, pair-independent factor, we have $\Xi_{\underline{0}\,i}^{1\kappa} \propto \frac{1}{\sqrt{2}} \sum_j U'_{ij}\, n_{ij}^{\kappa} = \underline{f}_i = \underline{0}$. Since such a proportionality is closely verified by Roskilde systems, especially LJ potentials, we expect the above equation to hold for these glasses as well.

APPENDIX D: COMPUTATION OF THE INDIRECT ELASTICITY TENSOR

As in Appendix C, we write the rank-3 tensor $\Xi_{\underline{k}\,i}^{\alpha\beta\kappa}$ as $\Xi_{\underline{k}\,i}^{a\,\kappa}$ with $a = 1, \ldots 4$. For any given a, $\Xi_{\underline{k}\,i}^{a\,\kappa}$ is a discrete vector field and [see Eq. (C1)]

$$\zeta_{n\,\underline{k}}^{a} = \Xi_{\underline{k}}^{a\,\dagger} \psi_n. \tag{D1}$$

Let us recall that the four-vector representation of rank-2 tensors used here is based on the Cartesian basis $(\underline{e}_x, \underline{e}_y)$. In this representation, the indirect elasticity tensor reads

$$\begin{aligned}\widehat{\mathcal{Z}}^{ab}(\omega, \underline{k}, \underline{k}') &= \sum_n \frac{\zeta_{n\,\underline{k}}^{a}\, \zeta_{n\,\underline{k}'}^{b\,*}}{\omega_n^2 - (\omega + i\eta)^2} \\ &= \Xi_{\underline{k}}^{a\,\dagger} \mathcal{G}^{\mathrm{np,np}}(\omega) \Xi_{\underline{k}'}^{b}.\end{aligned} \tag{D2}$$

Using this expression, the average indirect elasticity tensor may be immediately written in the time domain: $\langle \widehat{\mathcal{Z}}^{ab}(t, \underline{k}, \underline{k}) \rangle = \left\langle \Xi_{\underline{k}}^{a\,\dagger} \mathcal{G}^{\mathrm{np,np}}(t) \Xi_{\underline{k}}^{b} \right\rangle$. Note that since $\Xi_{\underline{k}}^{a\,*} = \Xi_{-\underline{k}}^{a}$ [Eq. (C2)], and since $\mathcal{G}^{\mathrm{np,np}}(t)$ is real, $\langle \widehat{\mathcal{Z}}^{ab}(t, \underline{k}, \underline{k}) \rangle$, being symmetric under inversion ($\underline{k} \to -\underline{k}$), is also real-valued. After numerical integration is this Cartesian representation, the tensor $\langle \widehat{\mathcal{Z}}^{ab}(t, \underline{k}, \underline{k}) \rangle$ is transformed into its radial form using Eq. (B7).

APPENDIX E: RETARDED INDIRECT COUPLING AND NP RESPONSE TO A DIPOLE

Let us define an atomic scalar field $\boldsymbol{\rho}^{(ij)}$ with the value

$$\rho_l^{(ij)} = \delta_{il} - \delta_{jl} \tag{E1}$$

on atom l. For any vector $\underline{f}$, the field $\boldsymbol{\rho}^{(ij)}\underline{f}$ is the discrete vector field corresponding to the force dipole $\pm\underline{f}$ on the pair (i, j). The response of the NP subspace to such a dipolar field

$$\mathbf{u}^{\mathrm{np}}(\omega) = \mathcal{G}^{\mathrm{np,np}}(\omega)(1 - \mathcal{P})\boldsymbol{\rho}^{(ij)}\underline{f} \tag{E2}$$

is linear in the components of $\underline{f}$. Hence, it can be written as

$$\underline{u}_l^{\mathrm{np}}(\omega) = \underline{\underline{\Gamma}}_l^{(ij)}(\omega) \cdot \underline{f}, \tag{E3}$$

where $\underline{\underline{\Gamma}}_l^{(ij)}(\omega)$ is a Green function describing the NP response at any point l to a source dipole on the pair (i, j). Let us recall that the dot denotes the contraction over Cartesian indices. $\underline{\underline{\Gamma}}_l^{(ij)}(\omega)$ reads explicitly

$$\Gamma_l^{(ij)\,\alpha\beta} = \left[\mathcal{G}^{\mathrm{np,np}}(\omega)(1 - \mathcal{P})\right]_{lm}^{\alpha\beta} \rho_m^{(ij)}. \tag{E4}$$

The force field induced, in NP, by a P plane wave displacement $\boldsymbol{\varphi}_{\underline{k},\underline{a}}$ is $-\mathcal{H}^{\mathrm{np,p}}\boldsymbol{\varphi}_{\underline{k},\underline{a}} = -(1 - \mathcal{P})\mathcal{H}\boldsymbol{\varphi}_{\underline{k},\underline{a}}$. It is the NP projection of $-\mathcal{H}\boldsymbol{\varphi}_{\underline{k},\underline{a}}$, which can be written as a sum of dipoles,

$$-\mathcal{H}\boldsymbol{\varphi}_{\underline{k},\underline{a}} = \sum_{i<j} \boldsymbol{\rho}^{(ij)} \underline{f}_{\underline{k},\underline{a}}^{(ij)}, \tag{E5}$$

where for each pair (i, j),

$$\underline{f}_{\underline{k},\underline{a}}^{(ij)} = -\frac{1}{\sqrt{N}} \underline{\underline{M}}_{ij} \cdot \underline{a} \left(e^{i\underline{k}\cdot\underline{r}_j} - e^{i\underline{k}\cdot\underline{r}_i} \right) \tag{E6}$$

is the force exerted by j onto i. Note that the force exerted by i on j is $\underline{f}_{\underline{k},\underline{a}}^{(ji)} = -\underline{f}_{\underline{k},\underline{a}}^{(ij)}$, as required by Newton's second law.

With these notations, we may now write

$$\begin{aligned}\mathcal{G}^{\mathrm{np,np}}(\omega)\mathcal{H}^{\mathrm{np,p}}\boldsymbol{\varphi}_{\underline{k},\underline{a}} &= \mathcal{G}^{\mathrm{np,np}}(\omega)(\mathbf{1} - \mathcal{P})\mathcal{H}\boldsymbol{\varphi}_{\underline{k},\underline{a}} \\ &= -\sum_{i<j} \mathcal{G}^{\mathrm{np,np}}(\omega)(\mathbf{1} - \mathcal{P})\boldsymbol{\rho}^{(ij)} \underline{f}_{\underline{k},\underline{a}}^{(ij)},\end{aligned} \tag{E7}$$

and then using Eqs. (E2) and (E3),

$$\left(\mathcal{G}^{\mathrm{np,np}}(\omega)\mathcal{H}^{\mathrm{np,p}}\boldsymbol{\varphi}_{\underline{k},\underline{a}}\right)_l = -\sum_{i<j} \underline{\underline{\Gamma}}_l^{(ij)}(\omega) \cdot \underline{f}_{\underline{k},\underline{a}}^{(ij)} \tag{E8}$$

Observe now that when computing the retarded coupling,

$$\begin{aligned}\widehat{Q}_{\underline{k},\underline{a},\underline{k}',\underline{a}'}(\omega) &= \boldsymbol{\varphi}_{\underline{k},\underline{a}}^{\dagger}\, \mathcal{Q}(\omega)\, \boldsymbol{\varphi}_{\underline{k}',\underline{a}'} \\ &= \boldsymbol{\varphi}_{\underline{k},\underline{a}}^{\dagger}\, \mathcal{H}(1 - \mathcal{P})\mathcal{G}^{\mathrm{np,np}}(\omega)\mathcal{H}^{\mathrm{np,p}}\boldsymbol{\varphi}_{\underline{k}',\underline{a}'},\end{aligned} \tag{E9}$$

we can remove the $(1 - \mathcal{P})$ appearing in the last expression because, by construction, $\mathcal{G}^{\mathrm{np,np}}(\omega)\mathcal{H}^{\mathrm{np,p}}\boldsymbol{\varphi}_{\underline{k}',\underline{a}'}$ lies in the NP subspace. Using Eqs. (E5) and (E8), we then find

$$\begin{aligned}\widehat{Q}_{\underline{k},\underline{a},\underline{k}',\underline{a}'}(\omega) &= \left(\mathcal{H}\boldsymbol{\varphi}_{\underline{k},\underline{a}}\right)^{\dagger} \mathcal{G}^{\mathrm{np,np}}(\omega)\mathcal{H}^{\mathrm{np,p}}\boldsymbol{\varphi}_{\underline{k}',\underline{a}'} \\ &= \sum_l \sum_{m \neq l} \sum_{i<j} \left(\underline{f}_{\underline{k},\underline{a}}^{(lm)}\right)^{*} \cdot \underline{\underline{\Gamma}}_l^{(ij)}(\omega) \cdot \underline{f}_{\underline{k}',\underline{a}'}^{(ij)}.\end{aligned} \tag{E10}$$

Finally, after reorganizing indices, and using the relation $\underline{f}_{\underline{k},\underline{a}}^{(lm)} = -\underline{f}_{\underline{k},\underline{a}}^{(ml)}$, we obtain

$$\widehat{Q}_{\underline{k},\underline{a},\underline{k}',\underline{a}'}(\omega) = \sum_{l<m} \sum_{i<j} \left(\underline{f}_{\underline{k},\underline{a}}^{(lm)}\right)^{*} \cdot \left(\underline{\underline{\Gamma}}_l^{(ij)}(\omega) - \underline{\underline{\Gamma}}_m^{(ij)}(\omega)\right) \cdot \underline{f}_{\underline{k}',\underline{a}'}^{(ij)}, \tag{E11}$$

which, after using the explicit expression (E6) for the force dipoles, becomes

$$\widehat{Q}_{\underline{k},\underline{a},\underline{k}',\underline{a}'}(\omega) = \frac{1}{N}\sum_{l<m}\sum_{i<j}\underline{a}\cdot\underline{\underline{\mathcal{M}}}_{ijlm}(\omega)\cdot\underline{a}'\left(e^{-i\underline{k}\cdot\underline{r}_m}-e^{-i\underline{k}\cdot\underline{r}_l}\right)\times\left(e^{i\underline{k}'\cdot\underline{r}_j}-e^{i\underline{k}'\cdot\underline{r}_i}\right) \tag{E12}$$

with

$$\underline{\underline{\mathcal{M}}}_{ijlm}(\omega) = \underline{\underline{M}}_{lm}\cdot\left(\underline{\underline{\Gamma}}_l^{(ij)}(\omega)-\underline{\underline{\Gamma}}_m^{(ij)}(\omega)\right)\cdot\underline{\underline{M}}_{ij}. \tag{E13}$$

It is important to note that, in the above expression for $\widehat{Q}_{\underline{k},\underline{a},\underline{k}',\underline{a}'}(\omega)$, each of the last two factors vanishes linearly with $\underline{k}$ or $\underline{k}'$ in the long wavelength limit. This enables us to rewrite $\widehat{Q}_{\underline{k},\underline{a},\underline{k}',\underline{a}'}(\omega)$ as follows:

$$\widehat{Q}_{\underline{k},\underline{a},\underline{k}',\underline{a}'}(\omega) = \frac{1}{N}\sum_{l<m}\sum_{i<j}\underline{a}\cdot\underline{\underline{\mathcal{M}}}_{ijlm}(\omega)\cdot\underline{a}'\left(\underline{k}\cdot\underline{r}_{lm}\right)\left(\underline{k}'\cdot\underline{r}_{ij}\right)\times\frac{e^{-i\underline{k}\cdot\underline{r}_m}-e^{-i\underline{k}\cdot\underline{r}_l}}{i\underline{k}\cdot\underline{r}_{lm}}\left(\frac{e^{-i\underline{k}'\cdot\underline{r}_j}-e^{-i\underline{k}'\cdot\underline{r}_i}}{i\underline{k}'\cdot\underline{r}_{ij}}\right)^* \tag{E14}$$

since each of the last two fractions is well-behaved at all $\underline{k}$ and $\underline{k}'$. Using $N = \rho V$, this expression can finally be recast as Eq.(50), i.e.,

$$\widehat{Q}_{\underline{k},\underline{a},\underline{k}',\underline{a}'}(\omega) = \frac{1}{\rho V}a^\alpha k^\beta a'^\kappa k'^\chi\,\widehat{\mathcal{Z}}^{\alpha\beta\kappa\chi}(\omega,\underline{k},\underline{k}'), \tag{E15}$$

with

$$\widehat{\mathcal{Z}}^{\alpha\beta\kappa\chi}(\omega,\underline{k},\underline{k}') = \sum_{l<m}\sum_{i<j}\mathcal{M}^{\alpha\kappa}_{ijlm}(\omega)\,r^\beta_{lm}\,r^\chi_{ij}\,\frac{e^{-i\underline{k}\cdot\underline{r}_m}-e^{-i\underline{k}\cdot\underline{r}_l}}{i\underline{k}\cdot\underline{r}_{lm}}\times\left(\frac{e^{-i\underline{k}'\cdot\underline{r}_j}-e^{-i\underline{k}'\cdot\underline{r}_i}}{i\underline{k}'\cdot\underline{r}_{ij}}\right)^*. \tag{E16}$$

DATA AVAILABILITY

The data that support the findings of this study are available from the corresponding author upon reasonable request.

REFERENCES

[1] V. L. Gurevich, D. A. Parshin, and H. R. Schober, "On the theory of Boson peak in glasses," J. Exp. Theor. Phys. Lett. **76**, 553–557 (2002).
[2] W. Schirmacher, "Some comments on fluctuating-elasticity and local oscillator models for anomalous vibrational excitations in glasses," J. Non-Cryst. Solids **357**, 518–523 (2011).
[3] E. Maurer and W. Schirmacher, "Local oscillators vs elastic disorder: A comparison of two models for the Boson peak," J. Low Temp. Phys. **137**, 453–470 (2004).
[4] P. W. Anderson, B. I. Halperin, and C. M. Varma, "Anomalous low-temperature thermal properties of glasses and spin glasses," Philos. Mag. **25**, 1–9 (1972).
[5] W. A. Phillips, "Tunneling states in amorphous solids," J. Low Temp. Phys. **7**, 351–360 (1972).
[6] W. A. Phillips, "Two-level states in glasses," Rep. Prog. Phys. **50**, 1657–1708 (1987).
[7] G. Monaco and S. Mossa, "Anomalous properties of the acoustic excitations in glasses on the mesoscopic length scale," Proc. Natl. Acad. Sci. U. S. A. **106**, 16907–16912 (2009).
[8] A. Marruzzo, W. Schirmacher, A. Fratalocchi, and G. Ruocco, "Heterogeneous shear elasticity of glasses: The origin of the Boson peak," Sci. Rep. **3**, 1407 (2013).
[9] R. Busselez, T. Pezeril, and V. E. Gusev, "Structural heterogeneities at the origin of acoustic and transport anomalies in glycerol glass-former," J. Chem. Phys. **140**, 234505 (2014).
[10] S. Gelin, H. Tanaka, and A. Lemaître, "Anomalous phonon scattering and elastic correlations in amorphous solids," Nat. Mater. **15**, 1177–1181 (2016).
[11] W. Dietsche and H. Kinder, "Spectroscopy of phonon-scattering in glass," Phys. Rev. Lett. **43**, 1413–1417 (1979).
[12] G. Monaco and V. M. Giordano, "Breakdown of the Debye approximation for the acoustic modes with nanometric wavelengths in glasses," Proc. Natl. Acad. Sci. U. S. A. **106**, 3659–3663 (2009).
[13] G. Baldi, V. M. Giordano, G. Monaco, and B. Ruta, "Sound attenuation at terahertz frequencies and the Boson peak of vitreous silica," Phys. Rev. Lett. **104**, 195501 (2010).
[14] G. Baldi, V. M. Giordano, and G. Monaco, "Elastic anomalies at terahertz frequencies and excess density of vibrational states in silica glass," Phys. Rev. B **83**, 174203 (2011).
[15] B. Ruta, G. Baldi, F. Scarponi, D. Fioretto, V. M. Giordano, and G. Monaco, "Acoustic excitations in glassy sorbitol and their relation with the fragility and the Boson peak," J. Chem. Phys. **137**, 214502 (2012).
[16] G. Baldi, M. Zanatta, E. Gilioli, V. Milman, K. Refson, B. Wehinger, B. Winkler, A. Fontana, and G. Monaco, "Emergence of crystal-like atomic dynamics in glasses at the nanometer scale," Phys. Rev. Lett. **110**, 185503 (2013).
[17] G. Baldi, V. M. Giordano, B. Ruta, R. Dal Maschio, A. Fontana, and G. Monaco, "Anharmonic damping of terahertz acoustic waves in a network glass and its effect on the density of vibrational states," Phys. Rev. Lett. **112**, 125502 (2014).
[18] L. Wang, L. Berthier, E. Flenner, P. Guan, and G. Szamel, "Sound attenuation in stable glasses," Soft Matter **15**, 7018–7025 (2019).
[19] A. Moriel, G. Kapteijns, C. Rainone, J. Zylberg, E. Lerner, and E. Bouchbinder, "Wave attenuation in glasses: Rayleigh and generalized-Rayleigh scattering scaling," J. Chem. Phys. **151**, 104503 (2019).
[20] L. Hong, V. N. Novikov, and A. P. Sokolov, "Is there a connection between fragility of glass forming systems and dynamic heterogeneity/cooperativity?," J. Non-Cryst. Solids **357**, 351–356 (2011).
[21] L. Hong, V. N. Novikov, and A. P. Sokolov, "Dynamic heterogeneities, Boson peak, and activation volume in glass-forming liquids," Phys. Rev. E **83**, 061508 (2011).
[22] C. Rainone, E. Bouchbinder, and E. Lerner, "Pinching a glass reveals key properties of its soft spots," Proc. Natl. Acad. Sci. U. S. A. **117**, 5228 (2020).
[23] C. Caroli and A. Lemaitre, "Fluctuating elasticity fails to capture anomalous sound scattering in amorphous solids," Phys. Rev. Lett. **123**, 055501 (2019).
[24] S. N. Taraskin and S. R. Elliott, "Anharmonicity and localization of atomic vibrations in vitreous silica," Phys. Rev. B **59**, 8572–8585 (1999).
[25] Since our objective is to understand how to reconstruct the full system by recoupling the P and NP problems, we limit our investigation to $n \geq 6$, because the full system data were shown to be size-independent only under this condition.[10]
[26] J. Horbach, W. Kob, and K. Binder, "Structural and dynamical properties of sodium silicate melts: An investigation by molecular dynamics computer simulation," Chem. Geol. **174**, 87–101 (2001).
[27] H. R. Schober, "Vibrations and relaxations in a soft sphere glass: Boson peak and structure factors," J. Phys.: Condens. Matter **16**, S2659–S2670 (2004).
[28] O. Pilla, S. Caponi, A. Fontana, J. R. Gonçalves, M. Montagna, F. Rossi, G. Viliani, L. Angelani, G. Ruocco, G. Monaco, and F. Sette, "The low energy excess of vibrational states in v-SiO_2: The role of transverse dynamics," J. Phys.: Condens. Matter **16**, 8519–8530 (2004).
[29] H. Shintani and H. Tanaka, "Universal link between the Boson peak and transverse phonons in glass," Nat. Mater. **7**, 870–877 (2008).
[30] V. Mazzacurati, G. Ruocco, and M. Sampoli, "Low-frequency atomic motion in a model glass," Europhys. Lett. **34**, 681–686 (1996).
[31] P. B. Allen, J. L. Feldman, J. Fabian, and F. Wooten, "Diffusons, locons and propagons: Character of atomic vibrations in amorphous Si," Philos. Mag. B **79**, 1715–1731 (1999).
[32] H. R. Schober and G. Ruocco, "Size effects and quasilocalized vibrations," Philos. Mag. **84**, 1361–1372 (2004).

[33]H. Mizuno, H. Shiba, and A. Ikeda, "Continuum limit of the vibrational properties of amorphous solids," Proc. Natl. Acad. Sci. U. S. A. **114**, E9767–E9774 (2017).
[34]M. Shimada, H. Mizuno, and A. Ikeda, "Anomalous vibrational properties in the continuum limit of glasses," Phys. Rev. E **97**, 022609 (2018).
[35]E. Lerner, G. Düring, and E. Bouchbinder, "Statistics and properties of low-frequency vibrational modes in structural glasses," Phys. Rev. Lett. **117**, 035501 (2016).
[36]E. Lerner and E. Bouchbinder, "Effect of instantaneous and continuous quenches on the density of vibrational modes in model glasses," Phys. Rev. E **96**, 020104 (2017).
[37]A. Lemaître, "Inherent stress correlations in a quiescent two-dimensional liquid: Static analysis including finite-size effects," Phys. Rev. E **96**, 052101 (2017).
[38]A. Lemaître and C. Maloney, "Sum rules for the quasi-static and visco-elastic response of disordered solids at zero temperature," J. Stat. Phys. **123**, 415 (2006).
[39]J. C. Dyre, "Hidden scale invariance in condensed matter," J. Phys. Chem. B **118**, 10007–10024 (2014).
[40]R. D. Mindlin, "Second gradient of strain and surface-tension in linear elasticity," Int. J. Solids Struct. **1**, 417–438 (1965).
[41]M. Tsamados, A. Tanguy, C. Goldenberg, and J. L. Barrat, "Local elasticity map and plasticity in a model Lennard-Jones glass," Phys. Rev. E **80**, 026112 (2009).
[42]P. M. Derlet, R. Maass, and J. F. Loeffler, "The Boson peak of model glass systems and its relation to atomic structure," Eur. Phys. J. B **85**, 148 (2012).
[43]H. Mizuno, S. Mossa, and J.-L. Barrat, "Measuring spatial distribution of the local elastic modulus in glasses," Phys. Rev. E **87**, 042306 (2013).
[44]H. Mizuno, S. Mossa, and J.-L. Barrat, "Acoustic excitations and elastic heterogeneities in disordered solids," Proc. Natl. Acad. Sci. U. S. A. **111**, 11949–11954 (2014).
[45]The adiabatic scheme requires inverting the NP sub-block of the Hessian at each integration timestep; the adiabatic and local scheme demands a full diagonalization of the NP problem.